

Annual Review of Biophysics

Learning to Model G-Quadruplexes: Current Methods and Perspectives

Iker Ortiz de Luzuriaga,^{1,2} Xabier Lopez,^{2,4}
and Adrià Gil^{1,3}

¹CIC nanoGUNE BRTA, 20018 Donostia, Euskadi, Spain; email: a.gil@nanogune.eu

²Polimero eta Material Aurreratuak: Fisika, Kimika eta Teknologia, Kimika Fakultatea, Euskal Herriko Unibertsitatea, UPV/EHU, 20080 Donostia, Euskadi, Spain

³BioISI—Biosystems and Integrative Sciences Institute, Faculdade de Ciências, Universidade de Lisboa, 1749-016 Lisboa, Portugal; email: agmestres@fc.ul.pt

⁴Donostia International Physics Center, 20018 Donostia, Spain

Annu. Rev. Biophys. 2021. 50:209–43

First published as a Review in Advance on
February 9, 2021

The *Annual Review of Biophysics* is online at
biophys.annualreviews.org

<https://doi.org/10.1146/annurev-biophys-060320-091827>

Copyright © 2021 by Annual Reviews.
All rights reserved

Keywords

G-quadruplex, DNA, DFT, QM/MM, coarse grain, molecular dynamics

Abstract

G-quadruplexes have raised considerable interest during the past years for the development of therapies against cancer. These noncanonical structures of DNA may be found in telomeres and/or oncogene promoters, and it has been observed that the stabilization of such G-quadruplexes may disturb tumor cell growth. Nevertheless, the mechanisms leading to folding and stabilization of these G-quadruplexes are still not well established, and they are the focus of much current work in this field. In seminal works, stabilization was observed to be produced by cations. However, subsequent studies showed that different kinds of small molecules, from planar and nonplanar organic molecules to square-planar and octahedral metal complexes, may also lead to the stabilization of G-quadruplexes. Thus, the comprehension and rationalization of the interaction of these small molecules with G-quadruplexes are also important topics of current interest in medical applications. To shed light on the questions arising from the literature on the formation of G-quadruplexes, their stabilization, and their interaction with small molecules, synergies between experimental studies and computational works are needed. In this review, we mainly focus on *in silico* approaches and provide a broad compilation of different leading studies carried out to date by different computational methods. We divide these methods into two

ANNUAL
REVIEWS **CONNECT**

www.annualreviews.org

- Download figures
- Navigate cited references
- Keyword search
- Explore related articles
- Share via email or social media

main categories: (a) classical methods, which allow for long-timescale molecular dynamics simulations and the corresponding analysis of dynamical information, and (b) quantum methods (semiempirical, quantum mechanics/molecular mechanics, and density functional theory methods), which allow for the explicit simulation of the electronic structure of the system but, in general, are not capable of being used in long-timescale molecular dynamics simulations and, therefore, give a more static picture of the relevant processes.

Contents

1. INTRODUCTION	210
2. NONQUANTUM METHODS	214
2.1. Molecular Dynamics Simulations	214
2.2. Metadynamics	220
2.3. Coarse-Grained Methods	222
3. QUANTUM METHODS	225
3.1. Semiempirical Methods	225
3.2. Quantum Mechanics/Molecular Mechanics Methods	227
3.3. Density Functional Theory Calculations on Reduced Models	229
4. SUMMARY AND CONCLUSIONS	232

1. INTRODUCTION

G-quadruplexes are noncanonical secondary structures formed from nucleic acid sequences that are rich in guanine. The basic unit of these structures is known as a G-quartet or G-tetrad and consists of a square planar structure formed by four guanine bases, which interact via Hoogsteen hydrogen bonds (145) (**Figure 1**). Stacking of more than one G-tetrad forms the G-quadruplex (**Figure 2**). This stacking is produced in such a way that the O6 atoms of guanines are oriented to the center of the structure, and the resulting system has some tubular empty space in the center, which is called the ion channel. When an alkali metal cation is placed (68) in this ion channel, it may interact with up to eight O6 atoms; this coordination leads to the stabilization of the G-quadruplex. Moreover, from the guanines involved in the G-tetrads of the G-quadruplexes, various numbers of interspersing residues form loops that connect each G-tetrad plane. G-quadruplexes can be viewed and studied as monomeric structures that differ in tetrad number, strand polarity, loop topology, etc., or they can be studied as multimers that form higher-order structures, which can contain hundreds of G-quadruplex monomers (12, 87). To form the G-quadruplexes, the regular duplex DNA structure must open; once the helix is divided, the guanine-rich strand forms the G-quadruplexes. Although G-quadruplexes coming from a single strand are the most common structures, G-quadruplexes derived from up to four different strands have been found (122, 127, 138, 186).

G-quadruplexes have been associated with a large number of genomic functions, such as transcription and replication (61), and studies have revealed their presence in key regions of the human genome, such as promoters (150), untranslated regions (UTRs) (10), and telomeres (17). In the case of telomeres, the formation of telomeric G-quadruplexes has been shown to inhibit telomerase activity (46), which is responsible for maintaining the length of telomeres and is involved in 85% of cancers (110). This inhibition causes apoptosis of cancer cells and, since telomerase

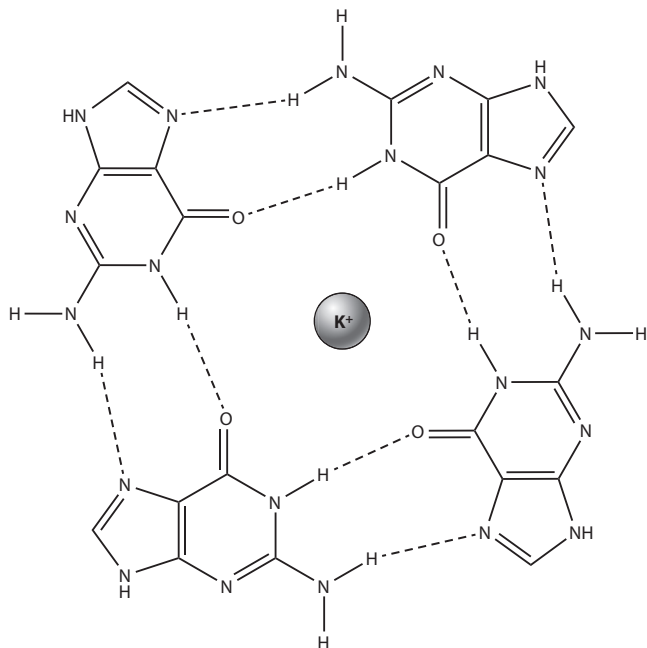


Figure 1

G-tetrad structure with a potassium cation.

is overexpressed in the majority of cancer cells and in relatively few somatic cells, is recognized as a potential cancer-specific target that would avoid the death of somatic cells in chemotherapy treatments for tumors. For this reason, this strategy has been considered in current drug design to devise alternative therapies for cancer treatments, and the studies on small molecules that bind and stabilize G-quadruplexes have become a current hot topic of pharmaceutical and medical research (43).

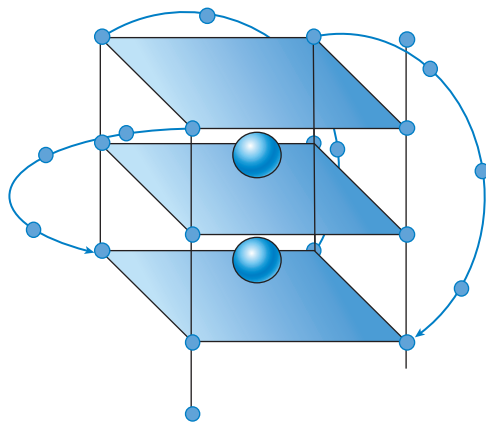


Figure 2

G-quadruplex structure formed by three stacked G-tetrads and metallic cations.

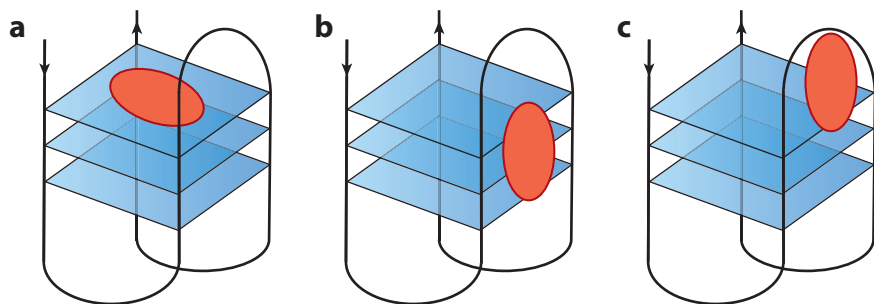


Figure 3

Representation of different binding modes between a ligand and a G-quadruplex DNA. (a) End stacking. (b) Groove binding mode. (c) Loop binding mode.

To both carry out the inhibition of telomerase and alter the expression of oncogenes via a mechanism similar to that described above, G-quadruplexes have to be stabilized to ensure the disruption of these processes. Many organic small planar molecules (2) and some metal complexes (22) showed not only high affinity for G-quadruplexes, but also more selectivity for binding to G-quadruplexes than to duplex DNA, indicating that they may further stabilize the G-quadruplexes. They may interact with G-quadruplexes by means of end stacking, groove binding, or the loop binding mode (**Figure 3**). The case of organic planar small molecules has been widely studied, and it has been shown that the following characteristics of the molecule increase the affinity for G-quadruplexes: (a) a π -delocalized system, which helps with the stacking of the G-tetrad; (b) a positive or partial positive charge, which interacts with the O6 of the guanines oriented toward the center of the G-tetrads; (c) positively charged substituents, which are able to interact with the negatively charged phosphate backbone; and/or (d) a surface area similar to the G-tetrads, which creates a greater affinity toward the G-quadruplex than toward regular DNA. Taking these characteristics into account, most of the studied ligands are organic molecules with a high number of aromatic rings, such as porphyrins, acridines, acridones, quinacridines, anthraquinones, porphyrazines, perylenes, quinoanthroxazines, barberines, bistriazoles, or coronenes. However, metal complexes offer a broad range of structural and electronic properties that can be exploited when designing new drugs. The metal center may be used as a structural focus to organize ligands in specific geometries and orientations for optimal G-quadruplex binding. In addition to their structural characteristics, the electronic properties of metal atoms may reduce the electron density on coordinated aromatic ligands. This allows the introduction of electron-poor systems, which are expected to show stronger π interactions with G-tetrads. Thus, although most of the reported molecules are purely organic structures, the interest in metal complex systems has increased during recent years. Below, we present some examples of molecules that are considered to be G-quadruplex stabilizers according to their structural features.

Porphyrins, which have wide aromatic surfaces, and their derivatives have been extensively studied. Substitutions at the meso position may possibly increase their selectivity and/or affinity to G-quadruplexes (67) (**Figure 4**). Metalloporphyrins were the earliest synthesized metal complexes due to the good results obtained with the pure organic porphyrins and the assumption that the introduction of a metal ion would add some electrostatic effects to the interaction that would enhance binding affinity. One of the most efficient porphyrin-based ligands is Mn^{III}-porphyrin, which can distinguish between duplex and G-quadruplex DNA by four orders of magnitude (38). Telomestatin is a natural macrocyclic compound that consists of seven oxazole rings and one thiazoline ring molecule and that has 70 times higher affinity for intramolecular G-quadruplexes than

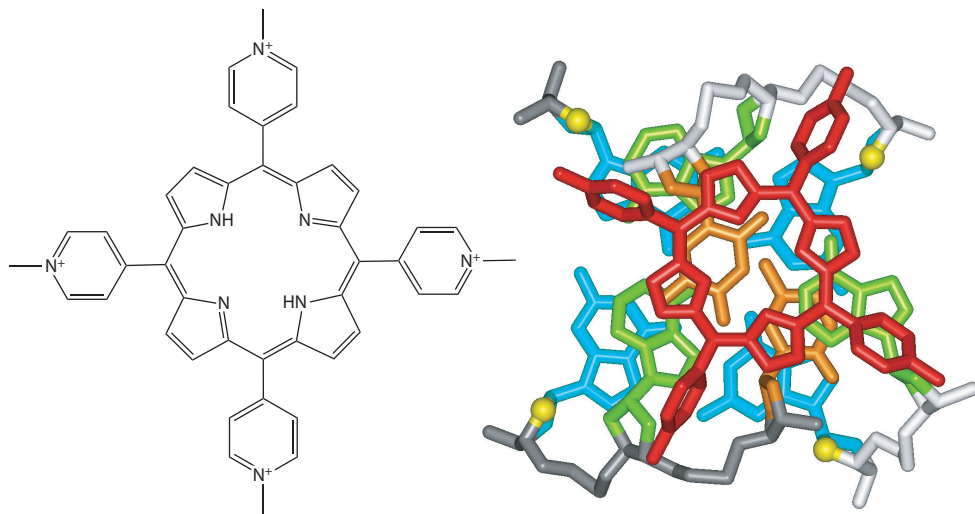


Figure 4

Chemical structure of TMPyP4 (*left*) and the overlapping of its porphyrin ring with terminal DNA bases (*right*).

for duplex DNA (83). Some compounds similar to telomestatin, such as hexaoxazoles or bistriazoles, have been shown to have a high degree of selectivity comparable to that of telomestatin and also exhibit moderate levels of cytotoxic activity (8, 111). Noncyclic polydentate compounds have also shown great potential to stabilize G-quadruplexes. One of the most studied complexes is the metal–salen system, which was able to intercalate between the DNA bases through π – π stacking (105) and has been studied using different metal centers and sidearms. Planar metal complexes made from combinations of Ni^{II}, Cu^{II}, and Pt^{II} metal atoms and both salphen and salen ligands were reported as efficient G-quadruplex binders (80, 166, 175). Nonplanar metal–salphen complexes, such as the Zn^{II}(H₂O)–salphen or the V^{IV}=O–salphen complexes (3), have also been considered, although such nonplanar complexes showed only low affinity or specificity and did not show effective G-quadruplex stabilization in general. Ru^{II}, Ir^{III} (129), and Fe^{III} (40) octahedral metal complexes with planar ligands have also been investigated, especially ruthenium polypyridyl complexes. The ligands that have given the best results for octahedral metal complexes are ethylenediamine (dien), bipyridine (bpy), phenanthroline (phen), dipyrrophenazine (dppz), phenanthroimidazol, and phenylpyridine (ppy) (25, 95, 96, 176, 180). In these octahedral metal complexes, it was observed that the planar ligands with large π -delocalized aromatic surfaces are involved in end-stacking or intercalating between DNA bases. However, it is more difficult for the nonplanar part of the molecule to interact at the end-stacking or its intercalation between DNA bases, which could become a problem for the achievement of an efficient interaction. Finally, some multinuclear metal assemblies have also been found to be effective G-quadruplex binders. Tetranuclear platinum(II), [Pt(en)(4,4'-dipyridyl)]⁴⁺, reported by Kieltyka et al. (82), was able to establish an effective interaction through end-stacking, where ethylenediamine ligands allowed hydrogen binding with the DNA backbones. The complex showed a strong stabilization of G-quadruplexes with high selectivity and telomerase activity inhibition [IC₅₀ = 0.2 μ M in an in vitro telomeric repeat amplification protocol (TRAP) assay]. There are also some di- and trinuclear Pt^{II} complexes that can achieve effective stabilization of G-quadruplexes (177, 178).

Thus, different molecules, binding modes, and mechanisms of stabilization of G-quadruplexes have been studied during the past decades with the aim of understanding and rationalizing the formation and stabilization of these G-quadruplexes. Nevertheless, much work has to be carried out to improve the use of G-quadruplexes as specific targets in alternative chemotherapies for cancer. In many of these investigations, experimental studies have been supported by computational methods for a better understanding of the formation of G-quadruplexes or their interaction with ligands. For this reason, knowledge of the state-of-the-art computational methods used in studies on G-quadruplexes is useful and timely. In this article, we carry out an extensive review of the state of the art of theoretical and computational methods used to address these systems; the review is divided into two parts: (a) nonquantum methods and (b) quantum methods. The former allows long-timescale molecular dynamics (MD) simulations, enhanced simulation techniques such as metadynamics, and the use of coarse-grained force fields. These methods can describe the evolution of the system over time and give highly relevant information on the dynamics of the system. The latter can be of different accuracy and efficiency and includes semiempirical, quantum mechanics (QM)/molecular mechanics (MM), and density functional theory (DFT) in reduced models. These types of methods can explicitly treat the electronic structure of the system. However, they have a limited application in terms of dynamic information, since, in general, they are computationally demanding and only allow short-time simulations. Therefore, they are used to provide a more static picture of the different interactions in the systems, characterized by accurate electronic structure determination. We expect that our work will be useful in classifying, compiling, and summarizing the state of the art of computational works applied to noncanonical DNA G-quadruplex structures and will help to improve new computational tools to be applied to this field of research with pharmaceutical and medical applications.

2. NONQUANTUM METHODS

2.1. Molecular Dynamics Simulations

Methods based on MD simulations have been the most-used computational methods for the study of G-quadruplexes and have the advantage of giving a view of the dynamic evolution of the system over time. The trajectories of the atoms composing the system are determined by solving the Newton's equations of motion numerically, whereas the forces between the particles and their potential energies are calculated by using interatomic potentials or molecular mechanical force fields. MD simulations are useful for studying G-quadruplexes because they accommodate the size of the structures and because no chemical reactions, in which covalent bonds are breaking and/or forming, have to be considered. In this context, the use of force fields is an appropriate choice to account for the energetics of a given structure of the system, but care should be taken to analyze the sensitivity of the calculations when using any specific force field.

Šponer, Orozco, and their colleagues (42) used side loops of G4-DNA as a benchmark to test the quality and accuracy of different force fields. They used Amber 5.0–9.0 software packages and CHARMM code to run and test several force fields [parm99 (24), parmbsc0 (125)], with a modified glycosidic χ torsion profile force field version done by Ode et al. (117) and CHARMM27 (47, 104). Side loops of systems were studied for the d(G4T4G4)₂ quadruplex from *Oxytricha nova* [OXY quadruplex; Protein Data Bank (PDB) ID 1JRN], which contains diagonal loops (58), and the human telomeric monomolecular d[AGGG(TTAGGG)]₃ quadruplex (HT quadruplex; PDB ID 1KF1) with propeller loops (122). They obtained many relevant results and conclusions. For instance, taking into account all of the calculations that were carried out, the behavior of the side chains did not change when the ion did, and the excess of salt did not seem to change the behavior of the side chains either. In addition to standard dynamics, locally enhanced sampling

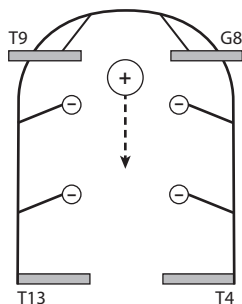


Figure 5

Scheme of ion penetration into the central binding site. Figure adapted with permission from Reference 135.

(LES) was run, which gave similar results. The importance of choosing a proper force field was also outlined. For instance, when using the parm99 force field, they were not able to reproduce experimental loop structures, the loops were unfolded, and the structure was lost. In contrast, using the parmbsc0 force field, the obtained loop structures were quite close to the experimental values and kept essentially identical geometries. However, the agreement with the experiment was not perfect. While, in the X-ray results, the adenine base is stacked with the first thymine of the loop, in the computational model, the adenine is stacked with its neighbor thymine in the loop due to the rotation of the first thymine. Modified parameters for χ torsion done at that time led to the same structures obtained with parm99 and parmbsc0 without χ modification; therefore, there was not any advantage to using the χ correction. In 2012, Krepl et al. (89) used χ torsion parameters, which significantly improved the G-quadruplex description and were also included in the current OL15 DNA force field.

Reshetnikov et al. (135) performed a study to address the ion binding and the ion penetration into the central ion channel of a 15-TBA G-quadruplex (**Figure 5**). They ran three different types of simulations: (a) 15-TBA, including K^+ or Na^+ ions, using the description of cations by pair-additive force fields (28); (b) the same system but with the TGT loop deleted; and (c) systems in which the two TT loops were removed. GROMACS 4.0 software was used for MD simulations with the parmbsc0 force field and TIP4P explicit solvent box with 15 Å depth from the solute. Negative charges of the system were neutralized by adding K^+ and Na^+ by replacing random water molecules in a distance equal to 6 Å, and in some simulations, an excess of salt was added. In the first type of simulation, Reshetnikov et al. observed that, in all simulations, the G-quadruplex spontaneously sucked the cation from the bulk, which finally reached the central ion channel. In that process, the G8 and T9 bases realigned to allow the access of the ion to the G-tetrads in a first step; subsequently, the guanines composing the G-quartet were forced to open to provide space to the cation to move to the final position in the center of the ion channel. **Figure 6** shows how the insertion of the Na^+ cation stabilizes the structure; however, in the case of K^+ , the ion took longer to be captured, and the G-quadruplex did not recover its structure before the end of the MD simulation. In the second type of simulation, where the TGT loop was removed, Reshetnikov et al. saw that the G-quadruplex was unable to keep the structure until the cation was trapped. In the third type of simulation, without TT loops, the structure collapsed in two out of 10 simulations. The capture of the ion occurred between 2 and 6 ns of the simulations, so it stabilized the structure. Reshetnikov et al. supported the work done with MD with QM/MM dynamics to demonstrate the relative stability of K^+ in different positions within the G-quadruplex structure. In this work, they saw how loops can influence the G-quadruplex geometry, stability, and ion binding, and that the TGT loop acted as a gate that allowed the ion to pass to the ion channel.

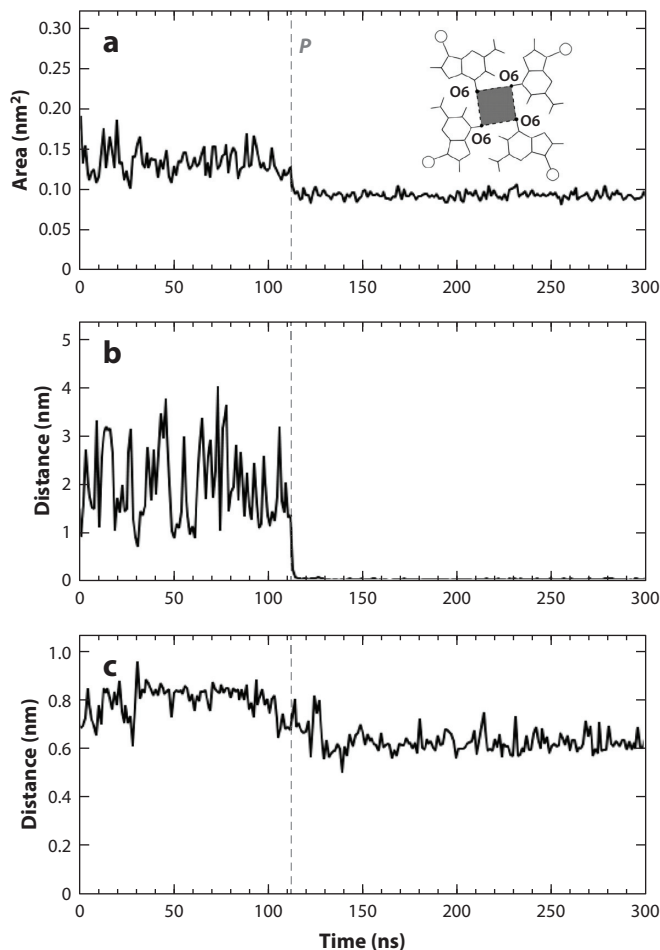


Figure 6

Molecular dynamics simulations of 15-TBA during Na⁺ penetration. The letter *P* in the figure and the dashed vertical lines indicate the simulation step where the cation penetrates the G-quadruplex. (a) Area of a square formed by O6 atoms of the upper G-quartet. (b) Distance between the cation and center of mass (COM) of the eight O6 atoms of the G-quadruplex. (c) Distance between the COMs of the G8 nucleic acid base and the eight O6 atoms of the G-quadruplex. Figure adapted with permission from Reference 135.

Petraccone and colleagues studied the interaction between 5,10,15-tris[4(1-piperidino)butyl]diindolo[3,2-a:3',2'-c]carbazole (azatrux) (51) and the 1KF1 G-quadruplex by docking and MD (126) simulations. For the docking, they used the INSIGHT II package (www.accerlys.com), calculating the partial charges for the azatrux molecule using MOPAC. Docking results indicated that the azatrux ligand docked on the 3'-end of the quadruplex. They hypothesized that the result was due to the orientation of the TTA loop, which created a groove accessible for the ligand, and the fact that the 5'-3' strand polarity generated by the phosphodiester backbone makes 3'-end more polar and favorable for the positively charged side chains of the ligand. For the MD simulations, the Amber parmbsc99 force field was used with the GROMACS package. The system was solvated in a TIP3P water box, and K⁺ counter-ions were added to neutralize the system. The simulations were run for 15 ns without any restriction on the system. The obtained root mean square

deviation (RMSD) from the simulation indicated that the azatrux-G-quadruplex complex was more stable than the G-quadruplex alone, with RMSDs of 2.3 Å and 2.7 Å, respectively. Moreover, the two side chains that are positioned in the groove, interacting with the ligand, maintained stable structures during the simulation, while the third chain, not interacting with the ligand, was highly flexible.

Islam et al. (71) studied the conformational variability of the TTA side loops. They used the 1KF1 PDB structure to model the G-quadruplex. The MD simulations were carried out using Amber11 software and the parmbsc0 version of the Cornell et al. (29) force field. The system was solvated in a TIP3P water box (65 Å × 64 Å × 68 Å). The integrity of the G-quadruplex was kept during the 1.5 μs of the MD simulations; to illustrate the importance of the timescale, RMSD was assessed over both short and long simulation times. As in most of the published systems, MD simulations were performed on a timescale from 1 to 100 ns. In this work, the authors wanted to show how different timescales provided different qualitative results of the dynamics. In fact, it was proven that, for the first approximately 300 ns of simulation, an ambiguous picture of the loop dynamics was obtained, and that only after that period of time was the system settled down. The root mean square fluctuation (RMSF) analysis indicated that the mobility of each of the loops was independent of the others, while at first it appeared to be equivalent, exposing again the relevance of the side chains and the influence that they could have on the stability of the system.

Grunenberg et al. (57) compared the performance of different force fields (AMBER, OPLS, MMFF) and DFT (ω B97XD) for two systems, *syn-anti* (SA) and *anti-anti* (AA). The work addressed a problem reported by Šponer et al. (155) in calculating different G-quadruplexes, where the force fields indicated that the SA stem was the lowest minimum (−14 kcal/mol with respect to the AA stem), whereas DFT favored the AA stem, 5 kcal/mol below the SA. In fact, this latter result agreed with the experimental evidence. Grunenberg et al.'s goal was to check the reliability of the force field calculations in G-quadruplex systems by testing different force fields to obtain the same results as DFT in both vacuum and solvation with water within a continuum approach. Grunenberg et al. found that both OPLS and MMFF force fields, but not AMBER, reproduced the experimental (and DFT) trend: higher stability for the AA stem in comparison with the SA stem. It must be said that their results were based on potential energy calculations in vacuum or considering a continuum approach for solvent effects, and it is known that, to evaluate a proper stability of any given system, the free energies must be taken into account, which requires an appropriate Boltzmann sampling. This Boltzmann sampling can only be attained by MD simulations in systems with a high number of degrees of freedom. One of the conclusions of this work is that the AMBER force field fails in the description of the relevant hydrogen bonds. Since G-quadruplexes are noncanonical DNA structures, and were not included in the original force field training set, the standard assignment of atomic charges is the source of small individual electrostatic errors. To solve this problem and reproduce the DFT results with AMBER, Grunenberg et al. modified the AMBER force field using quantum-adapted charges applying the Reppes and Goddards charge equilibrium (QE_q) formalism (131). The AMBER-QE_q force field indeed reproduced the experimental and DFT trends, and the AA rotamer was calculated to be the most stable conformer using the AMBER force field. The main conclusion of this work was that, whenever the empirical potential is flexible enough to adapt to special electrostatics, the force fields can reproduce the correct relative energy order of different arrangements of G-quadruplex guanine stems (G-DNA).

Barone et al. (165) extensively studied various salen- and Schiff-base metal complexes. They studied the affinity of three square-planar Ni^{II}, Cu^{II}, and Zn^{II} Schiff-base complexes [N,N'-bis-5-(triethyl ammonium methyl)-salicylidene-2,3-naphthalendiimine] for human telomeric (*h-telo*) and *c-myc* G-quadruplex (G4) DNA. They compared the results obtained experimentally

(with UV-visible absorption spectroscopy and circular dichroism) with molecular dynamics and QM/MM calculations. Schiff-base complexes were similar to salphen-base complexes but with an extended planar area. The absorption spectroscopy confirmed that the three metal compounds showed binding selectivity for G4 structures and that the binding of the Ni^{II} complex was tighter than that of Cu^{II}, which in turn was tighter than that of Zn^{II}. However, circular dichroism (CD) results indicated that Ni^{II} and Cu^{II} complexes had a preference to induce the formation of antiparallel *c-myc* G4 structures, whereas Zn^{II} stabilized the parallel structures. Furthermore, the Ni^{II} complex was able to induce the formation of G4-DNA, even in the absence of K⁺ cations. MD calculations were also performed between the Zn^{II} metal complex and *b-telo* and *c-myc*. The dynamics were run using GROMACS software with the Amber99 force field and parmbsc0 for nucleic acid torsion; K⁺ were considered as backbone phosphate group counter-ions. The results of the MD simulations showed that the strong interaction between the Zn^{II} complex and both G4-DNA models was driven by the strong electrostatic attraction between the positively charged triethylammoniummethyl groups of the Schiff-base ligand and the negatively charged phosphate groups of the biomolecule. In the case of *c-myc*, long-range interactions allowed the metal to easily approach the G-tetrad. Subsequently, π - π stacking interaction occurred, which brought the system to the equilibrium. However, in the case of *b-telo*, equilibrium was reached after 5 ns, and the metal complex remained stacked until the end of the MD simulations. The geometry after 50 ns was used for further geometry optimizations by hybrid ONIOM two-layer QM/MM calculations. The high layer involved the four guanine bases of the 3' ending of the G4-DNA and the metal complex; the rest of the system belonged to the low layer. It is interesting to see how the metal ion of the Schiff-base complex was aligned with the two potassium cations in the central channel formed by the three stacked G-tetrads. The binding of the ligand to DNA was always exothermic. However, both entropy and solvation had a destabilizing effect on the DNA binding energy. The formation free energy was always smaller than the formation enthalpy, indicating that the entropic contribution, in $\Delta G = \Delta H - T\Delta S$, was always negative. Finally, the calculated formation free energy values in solution, -34.6 , -14.4 , and -20.9 kJ/mol⁻¹ for Ni^{II}, Cu^{II}, and Zn^{II}, respectively, were in good agreement with the experimental values.

Stadlbauer et al. (158) carried out μ s-scale explicit solvent MD simulations for G-triplexes, which can participate in the folding pathway of G-quadruplexes. To build the triplexes, four different monomolecular structures were used, removing the first or the last G-strand and its adjacent loop: the X-ray structure of a parallel-stranded quadruplex (PDB: 1KF1) (122), two NMR 3 + 1 hybrid quadruplexes [PDB: 2GKU (101) and 2JPZ (33, 171)], and a NMR antiparallel basket type structure (PDB: 143D) (171). Stadlbauer et al. took into account three possible cation layouts: (a) one cation placed between the first and second G-tetrads, (b) one cation placed between the second and third G-tetrads, and (c) two cations filling the ion channel. Solute waters were added with the xLeaP module of Amber12 in a truncated octahedral box with a minimum distance of 10 Å from the solute. The TIP3P water model was used for the NaCl simulations, and the SCP/E model (78) was used for the KCl simulations. In all of the simulations, an excess of salt was added. The MD simulations were carried out with the CUDA version of the pmemd module of Amber12 (91) using the parmbsc0 version of the Cornell et al. (29) force field. Periodic boundary conditions were used, and electrostatic interactions were calculated by the Edwald method (34) with the nonbounded cut-off set to 9 Å. Furthermore, the 2-fs-step SHAKE algorithm (139) was applied to hydrogen-containing bonds to restrain the bond distances. They found that antiparallel triplexes with diagonal and lateral loops were potentially stable enough to keep the structure during a considerable amount of time and thus to be considered as part of the folding pathway of the complex G-quadruplex folding process. However, all parallel triplexes lost their structure within 10 ns, which is in agreement with the study done by Štefl et al. (160) showing instability of parallel-stranded

G-triplexes. More interesting was the case of antiparallel triplexes with two lateral loops. A rearrangement of side loops transformed the lateral loops to diagonal loops, a change that preserved the compatibility of the *syn/anti* distribution of the antiparallel triplex. Such strand reorientation could occur during the dynamics of real triplexes. Štefl et al. also studied a triplex with a fourth nonbonded G-strand. They carried out 5 μ s simulation to check if the unlinked chain joined the rest of the structure to form the G-quadruplex. Unfortunately, the rearrangement was unreachable on their μ s simulation timescale, and no noticeable movement of the strand was observed. Finally, they noticed that triplexes with narrow grooves between two of their strands attract cations from the bulk solvent into the groove, since the close space between the phosphates creates an electrostatic minimum inside the groove and an optimal space for the ion binding.

Barone et al. (20) studied a Ni^{II} and Zn^{II} salen-base complex with a small difference in the 2,3-diimine group, which was turned into a 4,5-pyrimidindiimine. MD simulations were run with the GROMACS 5.0.4 package, using the Amber99 force field parmbsc0. The simulation, of 250 ns, started with the metal complex 10 Å away from the 3' G-quartet, to simulate the molecular recognition process. The RMSD plot of the nonhydrogen atoms showed that G-quartets were rigidly bound around their equilibrium position during all simulation time. However, the large values of the RMSD of all atoms were due to the large and continuous oscillations of the highly flexible loops and surrounding bases. In agreement with previous works (165), during the simulation, the metal complex roughly aligns the nickel atom with the potassium channel. However, the metal is not equidistant from the four bases because of the presence and steric hindrance of the TTA loop.

Barone and colleagues (19) studied three Ni^{II} and Zn^{II} salphen-like ligands (N,N'-bis-salicylidene-1,2-phenylenediaminato) with different substituents (H, F, CF₃) in position 4 of the phenyl ring on the N,N' bridge. Ni^{II} complexes showed a higher affinity toward both duplex and G-quadruplex DNA compared to Zn^{II} analogs, but Zn^{II} complexes possessed high selectivity toward G-quadruplex DNA and a negligible affinity toward duplex DNA. Barone and colleagues (19) used a similar methodology to previous work (20), but instead of parmbsc0, they included the bsc1 correction (76). In the MD simulations with hydrogen as substituent group, the RMSD of the guanines remained stable, indicating that the general structure of the G-quadruplex kept its shape. However, in the RMSD of all atoms, a significant change could be seen between 200 and 400 ns (Figure 7). Barone et al. stated that this change corresponded to the movements of the TTA side loop. In any case, the principal structure and the distance between the metal complex and the G-quadruplex did not change. In the case of fluorine substituent, the system reached a

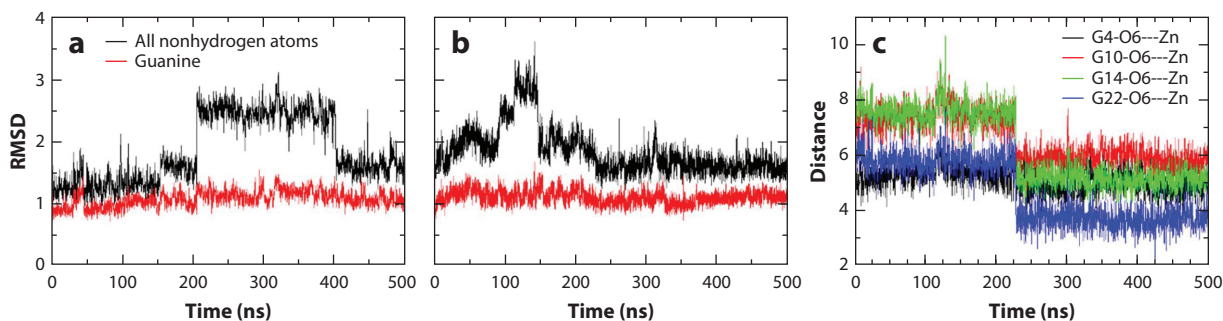


Figure 7

RMSD (Å) of all nonhydrogen atoms (*black*) and guanine atoms (*red*) for the molecular dynamics simulation on the interaction between N,N'-bis-salicylidene-1,2-phenylenediaminato (*a*) Ni^{II} and (*b*) Zn^{II} and (*c*) RMSD (Å) distances between Zn^{II} and O6 atoms of the four guanines in the 3' quartet. Figure adapted with permission from Reference 19. Abbreviation: RMSD, root-mean-square deviation.

state of equilibrium at approximately 220 ns of simulation (**Figure 7**). The RMSD of the guanine atoms remained stable throughout all of the simulation time, confirming that the major conformational changes were only due to the G-quadruplex loops and the rotation of the triethylammonium group. The calculated distance between the F atom and the O6 oxygen atom (**Figure 7**) of G22 (4.9 Å) was very similar to that reported for the crystallographic structure by Campbell et al. (21) (PDB ID 3QSC), 5.3 Å for the F atom. Campbell et al. concluded that electrostatic repulsion between F and O6 atoms made the π - π stacking interaction less tight. Nonetheless, the computational simulations suggested that the distance was too long for such electrostatic repulsion. This was confirmed by experimental results in which, when a fluorinated substituent was introduced, no loss of DNA-binding strength occurred, as would be expected in the case of repulsion.

As one can see from these simulations, the location of cations in G-quadruplex channels is key to the stability and structural properties of these systems. However, it is not always clear where to locate these ions, and long-timescale simulations would be needed to equilibrate the initial position of these cations if the positions are assigned randomly. In this sense, it is important to highlight the recent work by York and colleagues (50) using the OL15 (125) FF combined with the 3D-RISM molecular solvation theory in MD to create a predictive model for cation occupancy in G-quadruplex channels as a function of salt concentration. In their recent cutting-edge work, Islam et al. (72) used the OL15 force field to provide new insights into the limitations of the MD methods applied to G-quadruplexes. For instance, they demonstrated that, even with high-performance computers and using specialized enhanced sampling or the Markov state model, one cannot achieve quantitative convergence of the loop conformational space; furthermore, propeller loops are not correctly described, an issue that appears to be unsolvable with just dihedral reparameterizations. They also showed that simulations within the microsecond timescale are needed to investigate the conformational plasticity of the loops. A realistic description of the loops is also difficult to resolve due to the lack of enough experimental data, as the loops are significantly underdetermined in NOE-based ensemble-averaged experiments, and therefore, a direct unambiguous comparison of MD with NMR is not possible. Finally, Jiří Šponer's group (63, 75) showed how the performance of the current force fields is not as good as expected when they are used to carry out long simulations and remarked on the care that one should take in choosing a proper force field and interpreting the theoretical results.

In conclusion, in general, classical MD simulations are the most-used computational methods to understand the structure and stability of G-quadruplexes, since the study of large biological systems requires taking into account the evolution of the system during some period of time. MD simulations have been used not only to study the interaction of G-quadruplexes with ligands, but also to study the conformations of side loops, which are responsible for the different structures and behaviors of the G-quadruplexes. Finally, one has to be careful with the choice of the different force fields and the different parameters chosen to study the G-quadruplexes, since not all of the standard force fields with standard parameters can describe these noncanonical DNA structures correctly.

2.2. Metadynamics

Metadynamics simulations, first proposed by Laio & Parrinello (90), have also been used to explore the free energy surface of G-quadruplexes. The algorithm describes the system using a few collective variables. During the simulation, the location of the system in the space determined by the collective variables is calculated, and a positive Gaussian potential is added to the real energy landscape of the system. In this way, the system is pushed away from the previous point. During the simulation, more and more Gaussian functions are added until the system explores the full

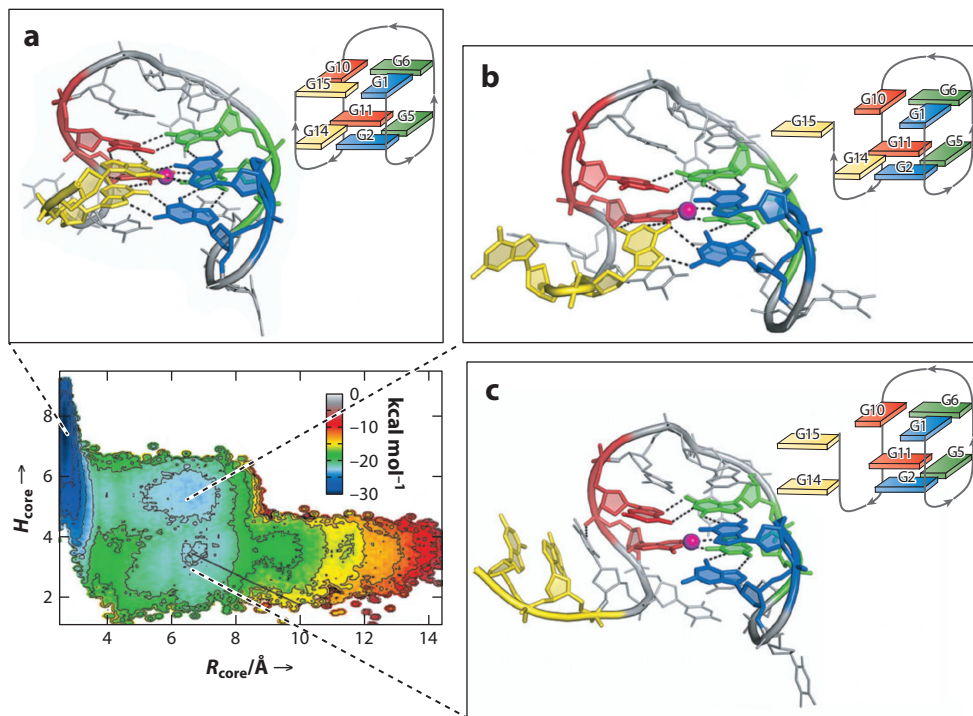


Figure 8

The free energy surface (FES) of the 3' end opening of TBA shows three main energy minima: (a) TBA occurs in the G-quadruplex structure, (b) an intermediate state occurs, and (c) the G-triplex structure is formed. Figure adapted with permission from Reference 96.

energy landscape. This method has been used to study the folding–unfolding processes and binding between ligands and G-quadruplexes.

Limongelli et al. (99) studied the unfolding pathway of the (5′-dGGTTGGTGTGGTTGG-3′) TBA G-quadruplex. The free energy surface (FES) was calculated as a function of two collective variables (CVs), the radius of gyration CV defined by the oxygen atoms of the guanines forming the G-tetrads and a second CV that counted the number of hydrogen bonds between these guanines. After approximately 80 ns of metadynamics simulation, three main energy minima were identified: (a) one that corresponded to the experimental TBA G-quadruplex structure (Figure 8a) (107); (b) a second that showed a partial opening of the 3′ end (Figure 8b) and can be considered the first event in the unfolding process of TBA; and (c) a third in which the 3′ end opens completely, with two guanine bases leaving the G-quartet (one guanine in each G-quartet) and pointing toward the solvent. The rest of the guanine bases formed a G-triplex. While the 3′ overhang was flexible, the rest of the TBA was rather stable, forming two G:G:G planes, namely, G-triads, that formed an array of Hoogsteen-like hydrogen bonds. In this conformation, the metal ion was coordinated at the center of the two triads in a similar way to that of the G-quadruplex structure. This G-triplex structure differed from the known triplex structures not only because of the base pairing, but also because of the conformation adopted by the side chains (Figure 9). The thermodynamic stability was investigated by CD. The spectrum showed two positive bands at 289 nm and 253 nm and two negative bands at 235 nm and 265 nm, indicative of a homopolar stacking of the nucleobases (130), in agreement with the proposed G-triplex structure.

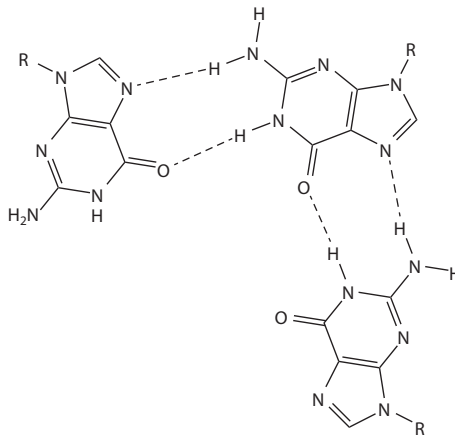


Figure 9

Representation of the G-triad structure for the G-triplex.

Bian et al. (16) studied the folding pathway of the hybrid-1 type human telomeric G-quadruplex. Four CVs were included in this case: (a) the total number of contacts between 12 guanines forming the G-tetrads (Q), (b) the dRMSD of the carbon atoms of the backbone, (c) the binding and contacts between K^+ ions and O6 atoms of guanines (N^{KO}), and (d) the radius of gyration (R^g). The free energy landscape (**Figure 10**) showed a diagonal shape, indicating cooperativity between the binding of metal ions and the formation of contacts between guanine bases. The proposed folding pathway started with intermediate-I at its unfolded state. Intermediate-II was characterized by a well-formed hairpin at the 3' terminal and an unstable hairpin at the 5' terminal. Intermediate-III corresponded to a triplex composed of the last three guanine steps, converging to the same conclusions obtained by Limongelli et al. (99). In intermediate-IV, two of the three G-tetrads were formed; at this folding stage, seven out of eight of the nearby nucleotides were in position, and thus one of the guanine bases was not docked. In the final two intermediates, the G-quadruplex was folded or almost folded. Bian et al. also studied the *syn/anti* orientations and observed that the bases took the correct orientations as long as they had a stable hydrogen bond, while the orientation *syn/anti* varied in the opposite case. Misfolded intermediates with wrong *syn/anti* configurations were observed in the early intermediates but not in the later ones.

These studies demonstrated the adequacy of metadynamics to explore the conformational space of these systems and allowed the determination of folding and unfolding pathways, which was not possible with standard MD techniques.

2.3. Coarse-Grained Methods

To perform long time simulations in complex biological systems like G-quadruplexes, we may use some approaches to simplify the description of the potential energy by using coarse-grained methods. Coarse-grained models (CGMs) were first presented by Levitt and Warshel (94, 172) and aim to simulate the behavior of complex systems by using their coarse-grained (simplified) representation. In coarse-grained models, the molecules are represented not by individual atoms but by pseudoatoms, which approximate groups of atoms such as the whole amino acid residue. By decreasing the degrees of freedom, one can study much longer simulation times at the expense of molecular detail.

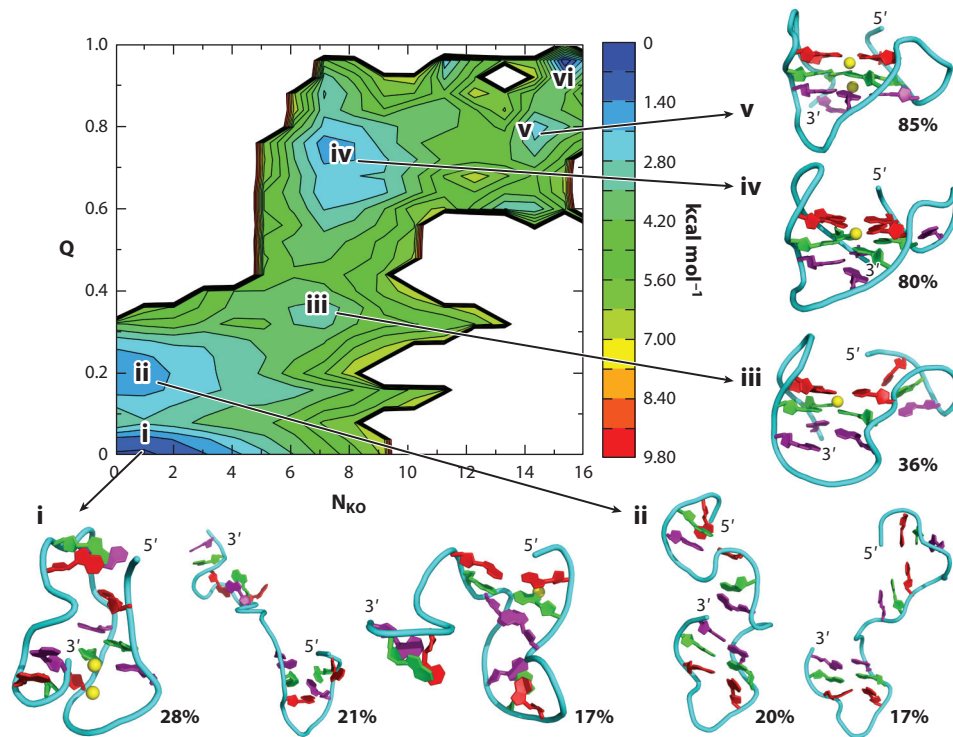


Figure 10

The free energy landscape and the representative structures of the basins of attraction. The units of the free energies are kcal mol⁻¹. Figure adapted with permission from Reference 16.

Rebic et al. (132) developed the first CGM for G-quadruplexes. The MagiC software package (112) was used to coarse-grain the reference system, 2HY9 (33) human telomeric [3+1] hybrid type with d[A₃G₃(T₂AG₃)₃A₂] sequence. The position of each CGM bead was calculated as the center of mass of the included atoms in each nucleotide or group, and the total charge of the atomic group was assigned as the charge of the bead. The reference molecule consisting of 843 atoms was reduced into a CGM system of 21 beads by taking each nucleotide and grouping them into a single bead (**Figure 11**). The model contained three types of beads, G-quadruplex core (G), loop (L), and potassium ions (K). To describe intermolecular interactions, three combinations had to be added, G–K, L–K, and K–K, since G and L are in the same fragment, and only K were not bounded. Based on a detailed core description, different combinations on G-tetrads were taken into account, which meant that different *syn/anti* bead arrangements could have different intermolecular bond interaction potentials. Additional bond interactions between G-strand beads were required to keep the proper distance between G-tetrad planes. Furthermore, the G beads and potassium ions interacted purely through the intermolecular pairwise interactions, while G beads and channel potassium interactions contained additional intramolecular terms; thus, it was necessary to describe the interaction between these two ions separately. Altogether, the reference structure interactions were described using 17 different effective potential terms, 3 of which were intermolecular, and 14 of which were intramolecular.

The MagiC's kernel module was used to obtain the effective CGM potentials by means of the iterative Boltzmann inversion (IBI) (154) and inverse Monte Carlo (IMC) (103) methods, also

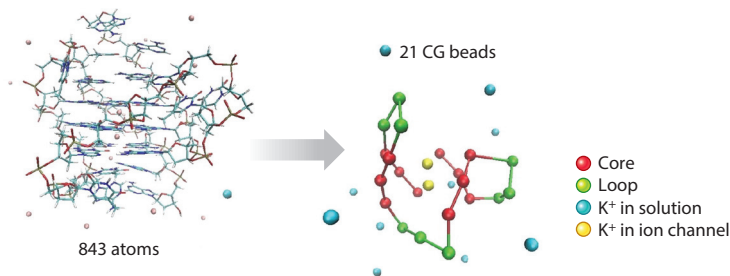


Figure 11

Mapping scheme used to generate the coarse-grained model. Red indicates the core, green indicates the loop, cyan indicates K^+ in solution, and yellow indicates K^+ in the ion channel. Figure adapted with permission from Reference 132.

known as Newton inversion (NI) (102). The software, through an iterative process, refined the effective potentials and fitted them to reproduce the intermolecular and intramolecular distances and angles. Inspection of the RMSF revealed that the guanine residues constituted a rigid block during the whole simulation ($1 \mu\text{s}$), and their fluctuations were within 1 \AA from the reference experimental structure. A structure of 20 blocks of 1KF1 parallel G-quadruplex was also built in which the blocks were consecutively stacked on each other and interacted purely through the G-tetrads (no TTA loop between blocks and terminal G beads of blocks were connected in the $5' \rightarrow 3'$ direction) (**Figure 12**). The structure was mapped using the same rules as for 2HY9. Rebic et al. (132) observed that the G-tetrads of the higher-order structure did not change the behavior from that observed in the small 1KF1 building block. To study the structure flexibility, the calculated RMSF with respect to starting G beads was compared; the fluctuation profile of the G-quadruplex showed a similar trend as a CGM of canonical DNA (115).

Stadlbauer et al. (157) studied the unfolding of human telomeric G-quadruplexes using coarse-grained methods. In this case, simulations were performed using HiRE-DNA (31) where, instead of using one bead (132) for each nucleotide, the authors used six or seven beads, corresponding to the backbone-heavy atoms P, O5', C5', C4', and C1', and to the center of mass of each of the aromatic rings of the bases (**Figure 13**). Geometric parameters controlling bond distances,

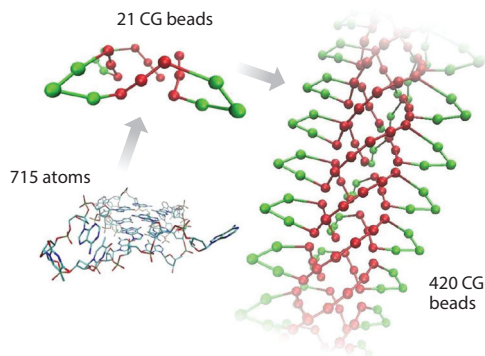


Figure 12

Reduction of degrees of freedom for the 1KF1 and the structure consisting of 20 blocks of 1KF1. The structure is shown without potassium ions. Figure adapted with permission from Reference 132. Abbreviation: CG, coarse-grained.

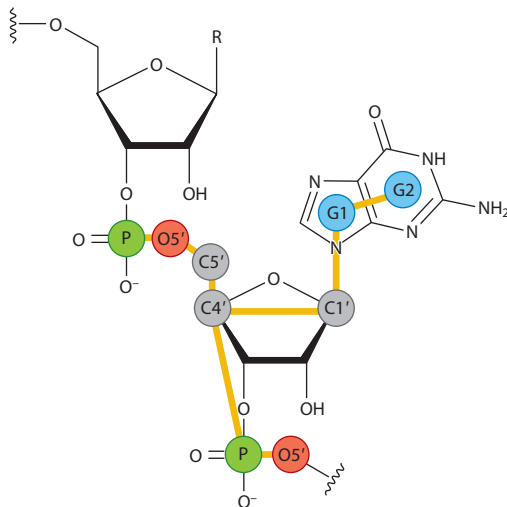


Figure 13

Coarse-grained model representation of a guanine nucleotide. Figure adapted with permission from Reference 157.

equilibrium angles, and dihedrals were specific for each type of nucleotide (A, G, C, U). CGM simulations were carried out for five structures, each with different *syn/anti* orientations: 1KF1, 143D, 2JSM (127), 2KF8 (98), and 2KM3 (97). In most cases, the unfolding came from destabilization of one terminal G-tetrad, which caused a loss of stacking, and the unpaired bases were oriented toward solvent. After the first destabilization, the unfolded G bases were free to fluctuate between *syn* and *anti* conformations, and finally, all structure was destabilized. In the case of 2JSM, a short-living G-triplet structure was formed, in agreement with other studies (16, 99).

In summary, coarse-graining provides the critical link between the highly detailed world of the atomic interactions and the highly averaged world of thermodynamics. In many ways, CGMs complete the quest to use computer simulation and molecular modeling to understand and predict the behavior of biomolecular systems. In the case of G-quadruplexes, coarse-grained methods make it possible to study larger systems on a longer timescale, which is always beneficial in biological systems.

3. QUANTUM METHODS

In the previous section, we describe how quantum methods can be applied to improve the force fields, especially atomic charges, which are then applied to perform MD simulations. In addition, quantum methods can also be used to gain insight into the thermodynamics and structural details of G-quadruplexes and their various chemical properties. In this section, we discuss some of the work on this subject.

3.1. Semiempirical Methods

Semiempirical quantum chemical methods gain speed in their implementation over computers by neglecting many of the difficult integrals (such as several two-electron integrals) that appear with the application of first-principles methods to molecular problems. The error introduced using semiempirical models is compensated with the use of parameters determined by the comparison

of calculations with experiments, which requires careful parameterization. This procedure can sometimes produce a model of higher accuracy when compared to the experiment than can *ab initio* calculations. There are currently several kinds of software with different approximations depending on the goal to be achieved. MOPAC, AMPAC, and SPARTAN use parameters to fit experimental heats of formation, dipole moments, ionization potentials, and geometries. There are also methods whose primary aim is to calculate excited states and thus to predict electronic spectra. These methods include ZINDO (184) and SINDO (114).

Semiempirical methods are mainly used to calculate partial charges (14) to improve force fields that are then used in MD simulations (59, 60, 126). However, some works use semiempirical methods to gain relevant information on the thermodynamics and structural properties of the systems of interest. In this section, we highlight some relevant works with this purpose in the field of G-quadruplex research.

Husby et al. (70) developed a systematic and general approach to determine all plausible positions for binding a ligand to a G-quadruplex structure (dynamic docking), taking fully into account the flexibility of both the target [1K8P, parallel-folded intramolecular human telomeric quadruplex (122)] and the ligands [pyridostatin (136) and the pentacyclic acridine derivative RHPS4 (143)]. They evaluated the most energetically favorable binding regions using three different methods to calculate free energies. They proposed three main steps: (a) sampling of the G-quadruplex and ligand conformational space via calculations of explicit MD starting from several ligand positions; (b) clustering of the ligand conformations determined by the MD calculations; and (c) calculation of binding energies of the proposed binding poses of the complexes using three different methods, one of them being the semiempirical PM6-DH2 method. Overall, they obtained a good correlation between methods, with a much better agreement between methods for pyridostatin compared to RHPS4. They observed that pyridostatin had some flexible ligands, and its conformational variability and electrostatic interactions with the backbones contributed to better binding and stabilization. They also found that pyridostatin had a slight preference of 4 kcal/mol for the 5' face compared to the 3' face of the G-quadruplex, while RHPS4 had no significant difference in the binding energies. Finally, they showed the better performance of their dynamic docking in comparison with conventional dockings, since their method was able to improve the description of the flexible side loops of the G-quadruplexes and the rotatable bonds of the ligands.

Semiempirical methods have also been used in G-quadruplexes to study other chemical properties. Dinçalp et al. (36) carried out a synthesis of binding studies and analysis of the visible absorption spectrum of Ph- β -GluOAc [4-O-(2,3,4,6-tetra-O-acetyl- β -D-glucopyranosyloxy)phenol] and PDI-Ph- β -GluOAc [N,N'-bis(2,6-diisopropylphenyl)-1,7-bis[4-O-(2,3,4,6-tetra-O-acetyl- β -D-glucopyranosyloxy)phenoxy]perylene-3,4,9,10-tetracarboxylic diimide] perylene diimide dyes. Theoretical calculations were performed using Hyperchem package v8.0 to characterize the geometries, visible spectra, and energy densities of the highest occupied molecular orbital (HOMO) and the lowest unoccupied molecular orbital (LUMO) surfaces of Ph- β -GluOAc by means of ZINDO/S. For the obtained HOMO-LUMO energy densities of the PDI-Ph- β -GluOAc molecule, the electronic distribution of the HOMO level was mostly centered in the core region of the molecule. The excited state did not show significant change in the charge distribution. Electron movement in $-C=C-$ linkages of the perylene ring led to single-component emission from the first excited state to the ground state. The simulated absorption spectrum of PDI-Ph- β -GluOAc and the experimental spectrum recorded in BzCN or MeOH solutions gave similar values. The small peak at 745 nm was assigned to the experimental recorded absorption peaks at 780 and 692 nm for BzCN and MeOH solutions, respectively. The main peak at 550 nm was assigned to the PDI chromophore absorption band experimentally recorded at 557 nm in MeOH solution.

Dinçalp et al. found that the simulated absorption spectrum gave values in agreement with the experimental spectrum in both BzCN and MeOH solutions. Moreover, due to PDI-Ph- β -GluOAc's affinity with G-quadruplexes, it might have utility in photodynamic therapy (PDT) applications.

3.2. Quantum Mechanics/Molecular Mechanics Methods

Because the QM treatment of an entire biological macromolecule requires very large amounts of computational time, and because MM methods cannot study bond formation and cleavage processes, hybrid QM/MM methods are commonly used to study chemical and biological processes in which an explicit treatment of electronic structure is needed for a localized part of the system. In this approach, a small region of the system where electronic structural changes are of interest is treated by means of QM, and the remaining part of the system (protein, DNA, solvent that is not involved in the reaction, etc.) is represented by some classical MM force field. Examples of this kind of problem include enzymes and ribozymes, where the description of the catalysis involves bond formation and cleavage (45, 146) that the force fields cannot take into account. The use of quantum methods for the description of part of the system is also required when the consideration of explicit electronic effects is needed for adequately accurate description of the properties of interest. For instance, quantum methods are needed when there are significant electronic polarization effects, important charge-transfer phenomena, or nonstandard nonbonded interactions such as atypical hydrogen bonds. In addition, the presence of high-valent metals could require a QM treatment due to the limitations of classical force fields in reproducing metal–ligand interactions. In this sense, QM/MM methods have been used for the study of G-quadruplexes, ligand–DNA interactions, side loop effects, and the effects of atom changes in nucleobases.

Terenzi et al. (165) used QM/MM methods combined with MD simulations to study the interaction of a Schiff-base ligand with three different metal centers (Ni, Cu, and Zn) and *b-Telo* G-quadruplexes (PDB ID 1KF1). For the QM/MM approach, they took into account the equilibrium geometry obtained from MD simulations after approximately 50 ns, and they used the ONIOM approach. The high layer involving the metal complex and the four guanine bases of the G-tetrads interacting with the ligand were treated at the M06-2X/dzvp level, whereas the rest of the system was treated with an Amber99 force field. Solvent effects were introduced by using the polarizable continuum model (PCM) (144) with the parameters corresponding to water. Optimized structures showed that the metal ion of the three complexes was in line with the two potassium ions in the central channel of the G4. Moreover, in the case of Cu and Zn, coordination occurred with one O6 of the G-tetrad. The geometry distortions and the coordination of the metal together with solvent and thermodynamic contributions explained the experimental data of the decreasing affinity order Ni > Cu \approx Zn. Standard enthalpy and Gibbs free energy were used to calculate in vacuo and in solution formation energies of the supramolecular complexes. The obtained binding energies were always exothermic, both in vacuo and in solution. However, both entropy and solvation had a destabilizing effect on the binding energy. The solvent destabilization decreased in the order Ni > Cu > Zn, in parallel with calculated APT charges. The role of the polar solvent could be rationalized by taking into account the considerable amount of electrostatic interactions in the binding. Furthermore, the formation free energy was always smaller than the formation enthalpy, both in vacuo and in solution, indicating that the entropic contribution was always negative. Finally, the calculated formation free energy values in solution, -34.6 , -14.4 , and -20.9 kJ/mol⁻¹, were in good agreement with the experimental values, -36.2 , -30.3 , and -30.2 kJ/mol⁻¹, respectively.

Aggrawal et al. (1) reported that replacing deoxyadenosine (dA) in the side loops with its oxidized form (8-oxo-7,8-dihydrodeoxyadenosine, OxodA) stabilized human telomeric

G-quadruplex DNA. They performed a geometry optimization by using the hybrid ONIOM QM/MM approach [B3LYP/6-31G(d):UFF], taking adenine bases at positions 8, 14, and 20 of the sequence (PDB ID: 2JSM) as the high-level layer and placing the rest of the sequences in the low-level layer. In the optimization, the geometries of the MM layer were frozen to avoid the introduction of errors from the force fields. Then, single-point (SP) calculations were carried out at the ONIOM[B3LYP/6-311++G(2d,p):UFF] level of theory. Their results indicated that the presence of OxidA in loops 2 and 3 (positions 14 and 20) stabilized the G-quadruplex DNA. This result was quite striking because the modification of the loops did not involve the G-quartet, which was thought to be a predominant factor in the stabilization of G-quadruplexes. The computational results indicated that the mutation of dA to OxidA was overall approximately 6.6 kcal/mol more stable.

Ferreira et al. (44) used QM/MM methods to study the interaction between two kinds of 9-amino acridines and some G-quadruplexes [PDB 2JWQ (66)]. In this study, the ligands and bases within 3.5 Å were taken as the high-level QM region, whereas the rest of the system was treated using the Amber force field. The boundary between the QM and MM parts was treated using the pseudo bond approach. Optimizations were run at the B3LYP/3-21G*:AMBER level. It was observed that the position of one of the 9-amino acridines was stabilized by four hydrogen bonds: two between the acridine hydrogen and N1A19 and N3A10 of 1.8 and 2.6 Å, respectively, and another between the carbonyl oxygen of the ligand and HN2G25 of 2.12 Å. Furthermore, the presence of the ligand induced a small clockwise 6 rotation of the A10 base, which led it to form an additional hydrogen bond with the T9 base while keeping all of its original hydrogen bonds. The position obtained for the second acridine was stabilized by six hydrogen bonds: three between the acridine hydrogen and N1A10, N2G11, and N7A17 of 3.1, 2.3, and 2.8 Å, respectively; another between the methyl piperazine hydrogen and OPA10 of 3.3 Å; another between the carbonyl oxygen and HN2G25 of 3.3 Å; and another between the acridine nitrogen and HN6A10 of 3.5 Å. Moreover, the interaction resulted in a clockwise rotation of 9 of the G11 base with respect to the original structure, allowing G11 to form two new hydrogen bonds with G26 and causing it to lose two of the four hydrogen bonds with G25. Overall, the second acridine [[9-[[2-(1H-Indol-3-yl)ethyl]amino]-4-acridinyl](4-methyl-1-piperazinyl)methanone] stabilized slightly more the G-quadruplex structure; the study was also able to explain the experimental differences in structural stabilities between the two 9-amino acridines.

UV radiation was also used to study the photochemical formation of cyclobutane pyrimidine dimers (CPDs), which are responsible for the majority of mutations induced by UV irradiation in mammalian cells (113, 181). CPDs induce a mechanism in which two consecutive bases on one strand bind together and discriminate the normal base-pairing of the double-strand structure in that area. This relatively rigid structure allows only for the formation of the *cis*, *syn* CPD isomer (152, 162). As G-quadruplexes have more flexible loops, which allow different orientations for the bases, an unusual formation of *anti* CPD has been observed in these structures. The phenomenon was studied by Lee et al. (93) using QM/MM. Two different structures were studied, 143D (171) and 2KF8, which led to basket type and form-3 type structures, respectively. In the QM/MM scheme, the ground state calculations were carried out using the BLYP/TZPP level of calculation, whereas the excited state calculations were performed at the ADC(2)/def2-SVP level of theory. The QM region included two thymine bases of two different TTA side loops (Thy5 and Thy17) and the adjacent guanine base. It was shown that the addition of guanine in duplex DNA helped in the formation of CPD through the charge-transfer (CT) state, where electrons were shifted from guanine to the adjacent thymine (92). Lee et al. did not include all of the guanines in the QM region; thus, the collective nature of guanine excited states (23) was not considered. The rest of the system was treated with MM using the Amberff99 force field with ff99bsc0 corrections. The

water molecules within 20 Å of Thy5 and Thy17 were kept, while the rest of the water molecules were discarded for efficiency. The link atom (147) scheme was used in the boundary between the QM layer and the MM layer. Finally, during the QM/MM optimization, the residues that were further than 10 Å from Thy5 and Thy17 were frozen. According to the obtained results, both *trans*, *anti* and *cis*, *syn* conformations could be formed. However, in the case of *cis*, *syn*, the two thymine bases were shown to be stacked on the top of the adjacent guanine (Gua3) and formed strong π stacking interactions, which facilitated CT from Gua3 to thymines. Therefore, the energy of the corresponding CT state was lower. However, the orientation of thymine and guanine bases in the Frank-Condon region prevented proper π stacking, resulting in higher energy of CT states, making *trans*, *anti* the dominant product. The simulations showed that the formation of *cis*, *syn* was energetically feasible, which was not observed by Smith et al. (152).

3.3. Density Functional Theory Calculations on Reduced Models

In DFT methods, the electronic structure of the system is considered by evaluating the electron density of the system instead of the electronic wave function. The advantage of DFT methods compared to semiempirical methods is that they are more accurate and do not depend on extensive parameterization. However, the main drawback is that they are still computationally expensive, and thus a full DFT treatment of any given system is currently limited to systems with a limited number of atoms. Therefore, systems including G-quadruplexes must be reduced to be studied at the DFT level. Usually, only the guanine bases of the G-quadruplexes are considered in these kinds of studies, and studies are mainly focused on analysis of the interaction between G-tetrads, as well as the interaction of G-tetrads with ions located in the ion channel.

One of the first works employing DFT was carried out by Clay et al. (26). To study the G-quadruplexes, they used the three G-tetrads and two ions of the ion channel of the 1KF1 (122) structure and removed the rest of the system. SP calculations and geometry optimizations were performed with Gaussian03 by using the Hartree-Fock method (only in the case of SP calculations) and the B3LYP functional, along with the 3-21G* and 6-31G** basis sets. For the SP calculations, Clay et al. considered three scenarios: (a) stacking of the three G-tetrads (12 guanines) with two ions, (b) the top G-tetrads with one ion, and (c) the bottom G-tetrad. The SP calculations were run for the replacement of the K⁺ ion with Na⁺ and also for the system without cations. The result was that stacked G-tetrads were more stable than individual G-tetrads. Surprisingly, they found that the systems with Na⁺ were approximately 20–40 kcal/mol more stable than those with K⁺, a result that was later proved to be wrong (183). In addition, several convergence problems were found for some optimizations. Nevertheless, the available optimized data supported the SP calculations in the conclusion that the structure without cations is not stable.

Gkionis et al. (52) performed a study comparing state-of-the-art DFT-D3 and MM methods when considering the binding of a single ion to two G-quartet layers and two ions to three G-quartet layers. They also employed continuum solvent models for both QM and MM. To prepare the stacked systems, initially, a four guanine tetrad was optimized using B3LYP/6-31G(d,p); then, the optimized tetrads were placed at an ideal distance of 3.4 Å with a helical twist of 45. Further optimizations were done keeping the G-tetrad geometries fixed and moving an ion (K⁺, Na⁺, or Li⁺) along the *z* axis of the ion channel (**Figure 14**). QM energies were obtained using the ORCA package (116) and evaluated using the TPSS meta-GG functional (159) enhanced by Grimme's dispersion correction (D3) with Becke-Johnson damping (56) and def2-TZVP all-electron Gaussian AO basis set (173); for the solvent calculations, the COSMO continuum solvation model was used. All MM energies were calculated using the AMBER12 package using the Cornell et al. (29) force field for the guanine bases, assigning a charge of 0.089 to the N9 hydrogen to neutralize

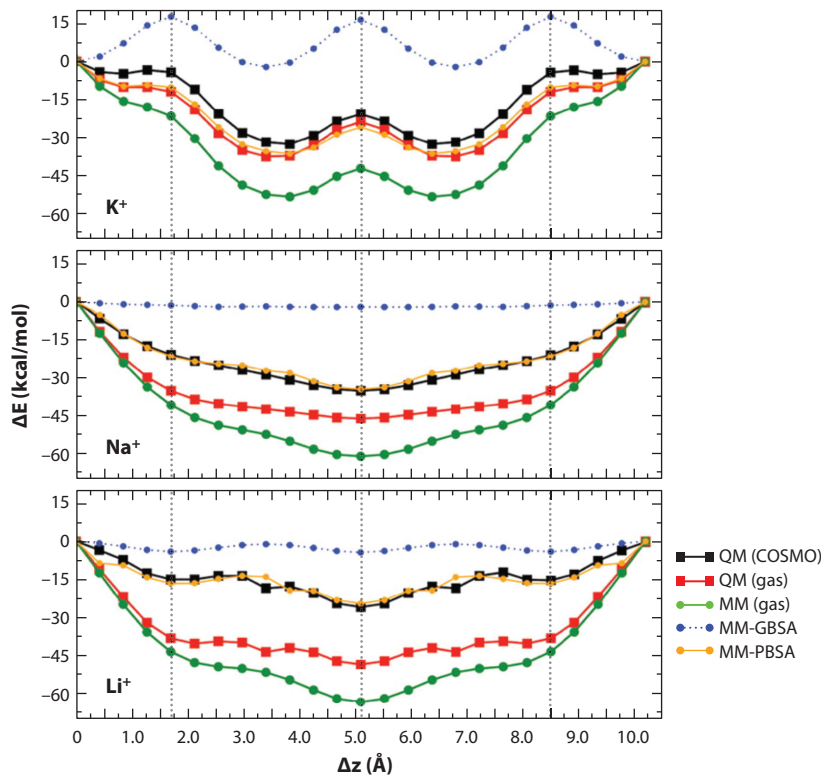


Figure 14

PES curves for three G-tetrad and one-ion system with K^+ , Na^+ , or Li^+ . The vertical lines mark passage of the ion through the quartet plane. Figure adapted with permission from Reference 52. Abbreviations: GBSA, generalized Born surface area; MM, molecular mechanics; PBSA, Poisson-Boltzmann surface area; PES, potential energy surface; QM, quantum mechanics.

the molecule. The ion parameters for TIP3P water were used for the description of the cations (79). Implicit solvation calculations were performed using generalized Born surface area (MM-GBSA) and Poisson-Boltzmann surface area (MM-PBSA) approaches. All of the MM calculations were carried out without periodic boundary conditions. To evaluate the potential energy surface, a scan was performed in which the cation was gradually pushed to the center of the cavity between G-tetrads, starting 1.7 Å from outside and moving 0.2125 Å with each step along the z axis. Furthermore, Gkionis et al. evaluated other systems apart from the system of two G-tetrads and one moving ion: two G-tetrads with two ions keeping one of them fixed, three G-tetrads stacking with one ion, three G-tetrads stacking with two ions keeping one fixed, and three G-tetrads stacking with two moving ions. In the case of three stacking systems, the ions moved 0.425 Å with each step. When one ion was moved, Gkionis et al. observed small differences between QM and MM in the gas phase, which is the binding that is most favorable at the MM level. The continuum solvent models gave the same results for QM (COSMO) and MM (PBSA) but showed inconsistencies with the GBSA solvation method. The results were reproduced with two and three G-tetrad layers (**Figure 14**). The addition of a second ion generated an overestimation of the intercation repulsion at the MM level due to the absence of polarization terms, reducing the electrostatic repulsion of the cations.

Fonseca Guerra et al. (48), after extensively studying the interactions between pairs of duplex DNA bases, shifted to the study of G-quadruplexes and focused on comparing two systems: a single guanine quartet and an adenine quartet. The calculations were run in gas phase and in aqueous solution by using dispersion-corrected DFT (DFT-D). This work had two objectives: (a) to study the stability of the G-quartet and (b) to observe if the A-tetrad maintained a flat structure without the stabilization provided by the π -stacking of an adjacent G-quartet. All of the calculations were done using Amsterdam Density Functional (ADF) (164) with different functionals: the generalized gradient approximation (GGA) functionals BLYP, BP86, and PBE; the dispersion-corrected variants BLYP-D, BP86-D, and PBE-D (55); and the M06-2X hybrid functional. Solvent effects in water were estimated by using the conductor-like screening model (COSMO) (85, 86). The results of BLYP-D showed that, in water, the quartet formed by guanines (G4) is the most strongly linked and is adopted more easily in a flat geometry. The flat geometries of all of the studied A4 quartets were significantly less stable than the flat G4 geometries. Furthermore, the more stable A4 structure was not flat. In other words, A4, unlike G4, had a strong tendency to adopt a geometry that was not suitable for stacking. This explained the fact that the A4 quartets have been experimentally observed in piles only between G4 quartets: They are less stable and not planar, and therefore, they need the stabilization of the flat G4 to form larger piles.

Fonseca Guerra et al. (49) also analyzed the telomeric DNA; they revealed that the cooperativity within the H-bonds is originated from the charge separation that comes from donor-acceptor orbital interactions in the σ -electron system, rather than from the strengthening caused by resonance in the π -electron system. They also demonstrated that guanine quartets were more strongly bounded than xanthine quartets (Xan4), even though they have the same number of hydrogen bonds. They explored these phenomena for larger aromatic complexes by substituting the NH hydrogen in the natural G-quartets with NX halogens (174). All calculations were performed with the ADF program and QUILD, using dispersion-corrected relativistic DFT at the ZORA-BLYP-D3(BJ)/TZ2P level for geometry optimizations and energies. The interaction energy in the hydrogen- and halogen-bonded model systems was examined using the so-called energy decomposition analysis (EDA), which splits the interaction energy into electrostatic contributions, Pauli repulsions, and orbital contributions, to which an extra term ΔE_{disp} was added to account for the dispersion interactions:

$$\Delta E_{\text{int}} = \Delta E_{\text{elstat}} + \Delta E_{\text{Pauli}} + \Delta E_{\text{oi}} + \Delta E_{\text{disp}}. \quad 1.$$

It was shown that, when going from fluorine to iodine bonds, the orbital interactions became more important due to lower acceptor orbital contributions to the halogen-donating fragment. This could lead to an even larger covalent character for halogen bonds than for the analogous hydrogen bonds and, consequently, a stronger cooperative effect. Moreover, they showed that, although alkali metal cations located in the central channel of G-quadruplexes weakened the hydrogen bonds, the synergy was kept in telomere-like structures.

Zaccaria et al. (183) analyzed the role of alkali metal cations in the stabilization of G-quadruplexes. Their general idea was to study the role of the alkali metal cation located between two quartets. It was thought that the reduction of the repulsion of the eight central oxygen atoms would enhance the hydrogen bond strength and stabilize quartet stacking. Computational analyses of double-layer guanine quartets and natural guanine G-quadruplexes with a sugar-phosphate backbone interacting with the monovalent cations (Li^+ , Na^+ , K^+ , Rb^+ , and Cs^+) were carried out. DFT-D was used at the ZORA-BLYP-D3(BJ)/TZ2P level. EDA was also considered to analyze the interaction between the cation and the guanines. In all cases, the most stable complex was the one with the potassium cation, consistent with the experimental findings. Moreover, computations revealed that the cation in the central cavity was not needed to compensate for the electrostatic

repulsion between the oxygen atoms of the guanines, as they do not repel each other. Nevertheless, this cation is needed for extra stabilization of the G-quadruplex.

Zaccaria & Fonseca Guerra (182) aimed to study the chemical–physical origins of the higher stability of RNA-GQ compared to DNA-GQ by using DFT-D and EDA. The energy linked to the formation of a structure without a cation from four ribonucleoside dimers explained how the formation of RNA-GQ was favored. The presence of an extra hydrogen bond involving the extra 2'-OH of the ribose of the RNA with the phosphate oxygen atoms gave higher conformational stability to the structure. Zaccaria & Fonseca Guerra also demystified the role of the cations in the self-assembly of G-quadruplex structures, disproving the general postulate that they minimize the repulsive forces between the oxygen atoms in the central channel and confirming their enthalpic relevance for thermodynamic stability.

4. SUMMARY AND CONCLUSIONS

In this review, we provide a global summary, compilation, and classification of the state-of-the-art computational works on G-quadruplexes. We focus especially on studies conducted to explain the formation and stabilization of G-quadruplexes and their interaction with ions and small molecules, particularly computational works and approaches used to treat such DNA systems. The most popular option for studying systems and processes involving DNA G-quadruplexes is MD simulations, for two main reasons. First, most ligand–DNA interactions are physical processes without chemical reactions, and it is known that the treatment of reactivity is one of the weak aspects of MD. Therefore, because the processes of stabilization of G-quadruplexes are not reactive from a chemical point of view, the use of MD simulations is, in principle, adequate. Second, G-quadruplex systems are relatively big, as are most biological systems. The use of MD simulations for this kind of system is common in the scientific community because, in exchange for losing precision, it allows one to study the entire system, taking into account evolution over time. When carrying out MD simulations, the Amber and GROMACS software with parm99 and parmbsc0 force fields have generally been used. However, we must be careful when using force fields. In general, the force field that has given the best results has been the parmbsc0. It must be said that these MD simulations may be complemented with QM/MM calculations to give a better description of the electronic structure of some important parts of the system and the interactions and/or processes occurring during the stabilization of G-quadruplexes. The QM/MM methods are considered to be the state of the art for systems in which a ligand interacts with DNA. MD simulations have been used in several studies aiming to reproduce the conformational variety of the loops. More work is needed in this area because of the lack of parameters and the performance of the current force fields. Šponer and colleagues (52, 63, 71, 75, 125, 135, 155, 158) have developed very useful and elegant work during the past years with the development and reparameterization of force fields, especially torsion parameters. Moreover, synergies between computational and experimental techniques are desired. Having enough experimental data and longer times for MD simulations will be very useful. MD simulations may be improved not only with the development of hardware and the use of GPUs, but also with the development of other methodologies, such as metadynamics. Coarse-grained methods also could achieve long times of simulation, but it is not obvious that they could solve the problem of the reproduction of the loops. MD simulations have also been the first choice to study the processes of folding and unfolding of these noncanonical secondary structures of DNA, in which the proper description of weak interactions plays a crucial role. As for the study of the loops, the choice of the force field is critical for a good description of these processes, and again, long time simulations are crucial for a proper description of the folding and unfolding processes in G-quadruplexes; the use of not only GPUs but also

alternative methods like metadynamics and coarse-grained methods could help and complement the classical and standard MD simulations. MD simulations have been used to study the stabilization of G-quadruplexes through interactions with ions and small molecules such as organic ligands and metal complexes. These works aiming to comprehend and rationalize the stabilization of G-quadruplexes through interaction with ions and small molecules are very common in the literature, and many studies aiming to comprehend and rationalize the interactions between ions and small molecules have appeared during the last years. These studies use not only MD simulation methods, but also QM/MM methods to complement the MD simulations. These kinds of studies, involving organic ligands and metal complexes, are very interesting from the pharmaceutical and medical points of view because, using the results and conclusions of these works, we could devise new small molecules employing substitution of ligands and changes in metals to improve the interactions and stabilization of G-quadruplexes. Thus, studies in the future on derivatives of these organic ligands and metal complexes could be very useful for pharmaceutical and medical applications. In this sense, an important aspect to take into account is not only the affinity of these small molecules with G-quadruplexes, but also the selectivity favoring their interaction with G-quadruplexes versus DNA duplexes. Affinities and selectivities of small molecules with DNA duplexes and G-quadruplexes have been analyzed with MD simulations and QM/MM approaches; noteworthy examples include the computational works of Barone and colleagues (19, 20, 57, 165, 166) and the experimental works of Neidle and colleagues (3, 27, 58–60, 73, 122), in which synergies with computational studies were found.

The state-of-the-art computational studies of G-quadruplexes have not been limited to the MD and QM/MM simulations; interesting DFT-D calculations about G-quadruplexes have been conducted on reduced models. These DFT-D methods can describe explicitly the electronic structure to give a more detailed picture of the molecule. However, they cannot deal with many atoms and the evolution of the system over time, which makes them incapable of describing the system in its complexity. This DFT-D choice was used especially by Fonseca Guerra and colleagues (48, 49, 174, 182, 183), who used reduced models of different numbers of G-tetrads to study the role of the ions in the channel, the stability of different kinds of G-quadruplexes (guanine versus adenine), and the cooperativity of the weak interactions (hydrogen bonds and stacking). One of the main conclusions obtained with this DFT-D approach was that alkali cations are not mandatory for the stabilization of G-quadruplexes, but their interactions with the DNA bases of the tetrads, when such alkali cations are inside the ion channel, give some extra stability to the system that helps to maintain the noncanonical secondary DNA structure. Another interesting finding obtained with reduced models and DFT-D computations was that RNA-G-quadruplexes may be more stable than the DNA-G-quadruplexes, a result that seems to be related to an extra hydrogen bond involving the 2'-OH of the ribose of the RNA with the phosphate oxygen atoms, which gives higher conformational stability to the structure. Finally, it is known that, since the inclusion of dispersion corrections in semiempirical methods, their application to large biological systems has been challenging. Unfortunately, few works have tried to apply semiempirical methods to the study of G-quadruplexes. These studies only calculated charges to be applied with other methods or studied the interaction of G-quadruplexes with some small molecules. However, some work by Dinçalp et al. (36) used semiempirical methods to study spectroscopic properties.

In summary, computational methods are generally able to reproduce the experimental evidence and help provide a better understanding of the processes involving G-quadruplexes. We must be careful when selecting methods, force fields, or other parameters that affect the simulations and quantum studies, since they can lead to results that are not correct. Even so, computational studies are a great complement to experimental studies and help to address with higher precision this important topic on the study of G-quadruplexes.

To give some perspective, as discussed above, we may consider the improvement of force fields and the improvement in the use of GPUs and alternative MD methods as metadynamics to enhance the exploration of potential energy surfaces and the use of coarse-grained methods to achieve longer times for MD simulations. We may also consider the use of QM/MD and/or QM/MM/MD by using large-scale DFT methods, like SIESTA, in which we could achieve longer times of simulations within a QM approach. Such QM/MD and QM/MM/MD simulations would consider the Boltzmann sampling obtained in classical MD simulations, with the extra point that they could give us important information on the electronic structure of the system (QM/MD) or part of the system (QM/MM/MD). Given the recent increase in the use of artificial intelligence applied not only to drug design but also to improving MD methods and QM methods, it could be interesting and challenging to study the opportunities that artificial intelligence could give us to improve studies on the formation, stabilization, and interaction of G-quadruplexes.

SUMMARY POINTS

1. Computational chemists mostly study the G-quadruplex side loop mobility, ligand interaction, and cation effects.
2. MD is the most-used method when studying G-quadruplexes because, in most cases, there is no reactivity, and it allow the user to simulate the entire system over time.
3. One has to be careful when choosing any force field, since it can dramatically influence the final results.
4. DFT-D methods have also been used in reduced models to study the stability of the G-quadruplexes, the weak interactions leading to their stabilization, and the interaction of G-quadruplexes with ions.

FUTURE ISSUES

1. G-quadruplex multimers are gaining attention in the scholarly community because there is evidence that G-quadruplexes can interact with each other when they are very close to each other (27, 32, 39, 60, 100, 133, 151, 169).
2. Current force fields are not fully prepared to simulate G-quadruplexes, and efforts are being made to improve them, for example, by adding polarization effects or torsion parameters (74).
3. It is important to highlight the large influence that the position and nature of cations have on the stability of G-quadruplexes. Predictive models for cation occupancy in G-quadruplex channels as a function of salt concentration (50) will gain importance for the proper simulation of these types of systems.
4. Methods and strategies are being developed to study G-quadruplexes through DFT in an optimized way. Batista and colleagues (5, 64) developed the moving-domain QM/MM method, and there is also software such as SIESTA capable of dealing with large systems using linear-scaling DFT for the full system (4, 118, 153).
5. It will be interesting to see how artificial intelligence is implemented in this field (11, 142).

DISCLOSURE STATEMENT

The authors are not aware of any affiliations, memberships, funding, or financial holdings that might be perceived as affecting the objectivity of this review.

ACKNOWLEDGMENTS

This research was financially supported by the Diputación Foral de Gipuzkoa through the Gipuzkoa Fellows Program to A.G. This research has also been financially supported by Fundação para a Ciência e a Tecnologia (FCT), project PTDC/QUI-QFI/29236/2017, and by the Spanish Ministry of Economy, Industry and Competitiveness under the Maria de Maeztu Units of Excellence Programme MDM-2016-0618. X.L. is also grateful for support from the Ministry of Science and Universities through the Office of Science Research (MINECO/FEDER; grants PGC2018-099321-B-I00) and Eusko Jaurlaritza, Spain (Ref. IT1254-19). I.O.d.L. is also very grateful to CIC nanoGUNE BRTA for his PhD grant.

LITERATURE CITED

1. Aggrawal M, Joo H, Liu W, Tsai J, Xue L. 2012. 8-Oxo-7, 8-dihydrodeoxyadenosine: the first example of a native DNA lesion that stabilizes human telomeric G-quadruplex DNA. *Biochem. Biophys. Res. Commun.* 421:671–77
2. Arola A, Vilar R. 2008. Stabilisation of G-quadruplex DNA by small molecules. *Curr. Top. Med. Chem.* 8:1405–15
3. Arola-Arnal A, Benet-Buchholz J, Neidle S, Vilar R. 2008. Effects of metal coordination geometry on stabilization of human telomeric quadruplex DNA by square-planar and square-pyramidal metal complexes. *Inorg. Chem.* 47:11910–19
4. Artacho E, Machado M, Sánchez-Portal D, Ordejón P, Soler JM. 2003. Electrons in dry DNA from density functional calculations. *Mol. Phys.* 101:1587–94
5. Askerka M, Ho J, Batista E, Gascón J, Batista V. 2016. The MOD-QM/MM method: applications to studies of photosystem II and DNA G-quadruplexes. *Methods Enzymol.* 577:443–81
6. Baguley BC. 2002. *A Brief History of Cancer Chemotherapy*. San Diego, CA: Academic
7. Balasubramanian S, Hurley LH, Neidle S. 2011. Targeting G-quadruplexes in gene promoters: a novel anticancer strategy? *Nat. Rev. Drug Discov.* 10:261–75
8. Barbieri CM, Srinivasan AR, Rzuczek SG, Rice JE, LaVoie EJ, Pilch DS. 2007. Defining the mode, energetics and specificity with which a macrocyclic hexaoxazole binds to human telomeric G-quadruplex DNA. *Nucleic Acids Res.* 35:3272–86
9. Baruah H, Barry CG, Bierbach U. 2004. Platinum-intercalator conjugates: from DNA-targeted cisplatin derivatives to adenine binding complexes as potential modulators of gene regulation. *Curr. Top. Med. Chem.* 4:1537–49
10. Beaudoin JD, Perreault JP. 2010. 5'-UTR G-quadruplex structures acting as translational repressors. *Nucleic Acids Res.* 38:7022–36
11. Belmonte-Reche E, Morales JC. 2020. G4-iM Grinder: when size and frequency matter. G-quadruplex, I-motif and higher order structure search and analysis tool. *NAR Genom. Bioinform.* 2:lqz005
12. Benito S, Ferrer A, Benabou S, Aviñó A, Eritja R, Gargallo R. 2018. Evaluation of the effect of polymorphism on G-quadruplex-ligand interaction by means of spectroscopic and chromatographic techniques. *Spectrochim. Acta A* 196:185–95
13. Bernadou J, Pratviel G, Bennis F, Girardet M, Meunier B. 1989. Potassium monopersulfate and a water-soluble manganese porphyrin complex, [Mn(TMPyP)](OAc)₅, as an efficient reagent for the oxidative cleavage of DNA. *Biochemistry* 28:7268–75
14. Besler BH, Merz KM Jr, Kollman PA. 1990. Atomic charges derived from semiempirical methods. *J. Comput. Chem.* 11:431–39

15. Bhattacharjee AJ, Ahluwalia K, Taylor S, Jin O, Nicoludis JM, et al. 2011. Induction of G-quadruplex DNA structure by Zn(II) 5,10,15,20-tetrakis(N-methyl-4-pyridyl)porphyrin. *Biochimie* 93:1297–309
16. Bian Y, Tan C, Wang J, Sheng Y, Zhang J, Wang W. 2014. Atomistic picture for the folding pathway of a hybrid-1 type human telomeric DNA G-quadruplex. *PLoS Comput. Biol.* 10:e1003562
17. Biffi G, Tannahill D, McCafferty J, Balasubramanian S. 2013. Quantitative visualization of DNA G-quadruplex structures in human cells. *Nat. Chem.* 5:182–86
18. Biswas PK, Gogonea V. 2005. A regularized and renormalized electrostatic coupling Hamiltonian for hybrid quantum-mechanical-molecular-mechanical calculations. *J. Chem. Phys.* 123:164114
19. Bonsignore R, Russo F, Terenzi A, Spinello A, Lauria A, et al. 2018. The interaction of Schiff Base complexes of nickel(II) and zinc(II) with duplex and G-quadruplex DNA. *J. Inorg. Biochem.* 178:106–14
20. Bonsignore R, Terenzi A, Spinello A, Martorana A, Lauria A, et al. 2016. G-quadruplex vs. duplex-DNA binding of nickel(II) and zinc(II) Schiff Base complexes. *J. Inorg. Biochem.* 161:115–21
21. Campbell NH, Karim NHA, Parkinson GN, Gunaratnam M, Petrucci V, et al. 2011. Molecular basis of structure–activity relationships between salphen metal complexes and human telomeric DNA quadruplexes. *J. Med. Chem.* 55:209–22
22. Cao Q, Li Y, Freisinger E, Qin PZ, Sigel RK, Mao ZW. 2017. G-quadruplex DNA targeted metal complexes acting as potential anticancer drugs. *Inorg. Chem. Front.* 4:10–32
23. Changenet-Barret P, Hua Y, Markovitsi D. 2015. Electronic excitations in guanine quadruplexes. In *Photoinduced Phenomena in Nucleic Acids II*, ed. M Barbatti, AC Borin, S Ullrich, pp. 183–201. Berlin: Springer
24. Cheatham TE III, Cieplak P, Kollman PA. 1999. A modified version of the Cornell et al. force field with improved sugar pucker phases and helical repeat. *J. Biomol. Struct. Dyn.* 16:845–62
25. Chen X, Wu JH, Lai YW, Zhao R, Chao H, Ji LN. 2013. Targeting telomeric G-quadruplexes with the ruthenium(II) complexes [Ru(bpy)(2+)(ptpn)](2+) and [Ru(phen)(2)(ptpn)](2+). *Dalton Trans.* 42:4386–97
26. Clay EH, Gould IR. 2005. A combined QM and MM investigation into guanine quadruplexes. *J. Mol. Gr. Model.* 24:138–46
27. Collie GW, Parkinson GN, Neidle S, Rosu F, De Pauw E, Gabelica V. 2010. Electrospray mass spectrometry of telomeric RNA (TERRA) reveals the formation of stable multimeric G-quadruplex structures. *J. Am. Chem. Soc.* 132:9328–34
28. Cordomi A, Edholm O, Perez JJ. 2009. Effect of force field parameters on sodium and potassium ion binding to dipalmitoyl phosphatidylcholine bilayers. *J. Chem. Theory Comput.* 5:2125–34
29. Cornell WD, Cieplak P, Bayly CI, Gould IR, Merz KM, et al. 1995. A second generation force field for the simulation of proteins, nucleic acids, and organic molecules. *J. Am. Chem. Soc.* 117:5179–97
30. Cosconati S, Marinelli L, Trotta R, Virno A, De Tito S, et al. 2010. Structural and conformational requisites in DNA quadruplex groove binding: another piece to the puzzle. *J. Am. Chem. Soc.* 132:6425–33
31. Cragolini T, Laurin Y, Derreumaux P, Pasquali S. 2015. Coarse-grained hire-RNA model for ab initio RNA folding beyond simple molecules, including noncanonical and multiple base pairings. *J. Chem. Theory Comput.* 11:3510–22
32. Cummario A, Fotticchia I, Franceschin M, Giancola C, Petraccone L. 2011. Binding properties of human telomeric quadruplex multimers: a new route for drug design. *Biochimie* 93:1392–400
33. Dai J, Carver M, Punchihewa C, Jones RA, Yang D. 2007. Structure of the hybrid-2 type intramolecular human telomeric G-quadruplex in K⁺ solution: insights into structure polymorphism of the human telomeric sequence. *Nucleic Acids Res.* 35:4927–40
34. Darden T, York D, Pedersen L. 1993. Particle mesh Ewald: an $N \log(N)$ method for Ewald sums in large systems. *J. Chem. Phys.* 98:10089–92
35. Dewar MJ, Thiel W. 1977. Ground states of molecules. 38. The MNDO method. Approximations and parameters. *J. Am. Chem. Soc.* 99:4899–907
36. Dinçalp H, Kirilok Ş, Birel ÖH, Içli S. 2012. Synthesis and G-quadruplex binding study of a novel full visible absorbing perylene diimide dye. *J. Photochem. Photobiol. A* 235:40–48
37. Dixon IM, Lopez F, Estève JP, Tejera AM, Blasco MA, et al. 2005. Porphyrin derivatives for telomere binding and telomerase inhibition. *ChemBioChem* 6:123–32

38. Dixon IM, Lopez F, Tejera AM, Estève JP, Blasco MA, et al. 2007. A G-quadruplex ligand with 10000-fold selectivity over duplex DNA. *J. Am. Chem. Soc.* 129:1502–3
39. Ducani C, Bernardinelli G, Högberg B, Keppler BK, Terenzi A. 2019. Interplay of three G-quadruplex units in the kit promoter. *J. Am. Chem. Soc.* 141:10205–13
40. Ebrahimi M, Khayamian T, Hadadzadeh H, Sayed Tabatabaei BE, Jannesari Z, Khaksar G. 2015. Spectroscopic, biological, and molecular modeling studies on the interactions of [Fe(III)-meloxicam] with G-quadruplex DNA and investigation of its release from bovine serum albumin (BSA) nanoparticles. *J. Biomol. Struct. Dyn.* 33:2316–29
41. Evans SE, Mendez MA, Turner KB, Keating LR, Grimes RT, et al. 2007. End-stacking of copper cationic porphyrins on parallel-stranded guanine quadruplexes. *J. Biol. Inorg. Chem.* 12:1235–49
42. Fadrná E, Spacková N, Sarzyńska J, Koca J, Orozco M, et al. 2009. Single stranded loops of quadruplex DNA as key benchmark for testing nucleic acids force fields. *J. Chem. Theory Comput.* 5:2514–30
43. Feng Y, Yang D, Chen H, Cheng W, Wang L, et al. 2016. Stabilization of G-quadruplex DNA and inhibition of Bcl-2 expression by a pyridostatin analog. *Bioorg. Med. Chem. Lett.* 26:1660–63
44. Ferreira R, Artali R, Benoit A, Gargallo R, Eritja R, et al. 2013. Structure and stability of human telomeric G-quadruplex with preclinical 9-amino acridines. *PLOS ONE* 8:e57701
45. Field MJ, Bash PA, Karplus M. 1990. A combined quantum mechanical and molecular mechanical potential for molecular dynamics simulations. *J. Comput. Chem.* 11:700–33
46. Fletcher TM, Sun D, Salazar M, Hurley LH. 1998. Effect of DNA secondary structure on human telomerase activity. *Biochemistry* 37:5536–41
47. Foloppe N, MacKerell AD Jr. 2000. All-atom empirical force field for nucleic acids: I. Parameter optimization based on small molecule and condensed phase macromolecular target data. *J. Comput. Chem.* 21:86–104
48. Fonseca Guerra C, van der Wijst T, Poater J, Swart M, Bickelhaupt FM. 2010. Adenine versus guanine quartets in aqueous solution: dispersion-corrected DFT study on the differences in π -stacking and hydrogen-bonding behavior. *Theor. Chem. Acc.* 125:245–52
49. Fonseca Guerra C, Zijlstra H, Paragi G, Bickelhaupt FM. 2011. Telomere structure and stability: Covalency in hydrogen bonds, not resonance assistance, causes cooperativity in guanine quartets. *Chem. Eur. J.* 17:12612–22
50. Giambaşu GM, Case DA, York DM. 2019. Predicting site-binding modes of ions and water to nucleic acids using molecular solvation theory. *J. Am. Chem. Soc.* 141:2435–45
51. Ginnari-Satriani L, Casagrande V, Bianco A, Ortaggi G, Franceschin M. 2009. A hydrophilic three side-chained triazatruxene as a new strong and selective G-quadruplex ligand. *Org. Biomol. Chem.* 7:2513–16
52. Gkionis K, Kruse H, Platts JA, Mladek A, Koca J, Šponer J. 2014. Ion binding to quadruplex DNA stems: comparison of MM and QM descriptions reveals sizable polarization effects not included in contemporary simulations. *J. Chem. Theory Comput.* 10:1326–40
53. Gonçalves DP, Rodriguez R, Balasubramanian S, Sanders JK. 2006. Tetramethylpyridiniumporphyrazines: a new class of G-quadruplex inducing and stabilising ligands. *Chem. Commun.* 45:4685–87
54. Gresh N, Naseem-Khan S, Lagardère L, Piquemal JP, Šponer JE, Šponer J. 2017. Channeling through two stacked guanine quartets of one and two alkali cations in the Li^+ , Na^+ , K^+ , and Rb^+ series: assessment of the accuracy of the SIBFA anisotropic polarizable molecular mechanics potential. *J. Phys. Chem. B* 121:3997–4014
55. Grimme S. 2004. Accurate description of van der Waals complexes by density functional theory including empirical corrections. *J. Comput. Chem.* 25:1463–73
56. Grimme S, Antony J, Ehrlich S, Krieg H. 2010. A consistent and accurate ab initio parametrization of density functional dispersion correction (DFT-D) for the 94 elements H-Pu. *J. Chem. Phys.* 132:154104
57. Grunenberg J, Barone G, Spinello A. 2014. The right answer for the right electrostatics: Force field methods are able to describe relative energies of DNA guanine quadruplexes. *J. Chem. Theory Comput.* 10:2901–5
58. Haider S, Parkinson GN, Neidle S. 2002. Crystal structure of the potassium form of an *Oxytricha nova* G-quadruplex. *J. Mol. Biol.* 320:189–200
59. Haider SM, Parkinson GN, Neidle S. 2003. Structure of a G-quadruplex–ligand complex. *J. Mol. Biol.* 326:117–25

60. Haider S, Parkinson GN, Neidle S. 2008. Molecular dynamics and principal components analysis of human telomeric quadruplex multimers. *Biophys. J.* 95:296–311
61. Hänsel-Hertsch R, Beraldi D, Lensing SV, Marsico G, Zyner K, et al. 2016. G-quadruplex structures mark human regulatory chromatin. *Nat. Genet.* 48:1267–72
62. Harrap K. 1985. Preclinical studies identifying carboplatin as a viable cisplatin alternative. *Cancer Treat. Rev.* 12:21–33
63. Havrila M, Stadlbauer P, Islam B, Otyepka M, Šponer J. 2017. Effect of monovalent ion parameters on molecular dynamics simulations of G-quadruplexes. *J. Chem. Theory Comput.* 13:3911–26
64. Ho J, Newcomer MB, Ragain CM, Gascon JA, Batista ER, et al. 2014. MOD-QM/MM structural refinement method: characterization of hydrogen bonding in the *Oxytricha nova* G-quadruplex. *J. Chem. Theory Comput.* 10:5125–35
65. Ho YP, Au-Yeung SC, To KK. 2003. Platinum-based anticancer agents: innovative design strategies and biological perspectives. *Med. Res. Rev.* 23:633–55
66. Hounsou C, Guittat L, Monchaud D, Jourdan M, Saettel N, et al. 2007. G-quadruplex recognition by quinacridines: a SAR, NMR, and biological study. *ChemMedChem* 2:655–66
67. Huang XX, Zhu LN, Wu B, Huo YF, Duan NN, Kong DM. 2014. Two cationic porphyrin isomers showing different multimeric G-quadruplex recognition specificity against monomeric G-quadruplexes. *Nucleic Acids Res.* 42:8719–31
68. Hud NV, Smith FW, Anet FA, Feigon J. 1996. The selectivity for K⁺ versus Na⁺ in DNA quadruplexes is dominated by relative free energies of hydration: a thermodynamic analysis by ¹H NMR. *Biochemistry* 35:15383–90
69. Huppert JL, Balasubramanian S. 2005. Prevalence of quadruplexes in the human genome. *Nucleic Acids Res.* 33:2908–16
70. Husby J, Todd AK, Platts JA, Neidle S. 2013. Small-molecule G-quadruplex interactions: systematic exploration of conformational space using multiple molecular dynamics. *Biopolymers* 99:989–1005
71. Islam B, Sgobba M, Laughton C, Orozco M, Sponer J, et al. 2013. Conformational dynamics of the human propeller telomeric DNA quadruplex on a microsecond time scale. *Nucleic Acids Res.* 41:2723–35
72. Islam B, Stadlbauer P, Gil-Ley A, Pérez-Hernández G, Haider S, et al. 2017. Exploring the dynamics of propeller loops in human telomeric DNA quadruplexes using atomistic simulations. *J. Chem. Theory Comput.* 13:2458–80
73. Islam B, Stadlbauer P, Krepl M, Havrila M, Haider S, Sponer J. 2018. Structural dynamics of lateral and diagonal loops of human telomeric G-quadruplexes in extended MD simulations. *J. Chem. Theory Comput.* 14:5011–26
74. Islam B, Stadlbauer P, Krepl M, Koca J, Neidle S, et al. 2015. Extended molecular dynamics of a c-kit promoter quadruplex. *Nucleic Acids Res.* 43:8673–93
75. Islam B, Stadlbauer P, Vorlicková M, Mergny JL, Otyepka M, Šponer J. 2019. Stability of two-quartet G-quadruplexes and their dimers in atomistic simulations. bioRxiv 820852. <https://doi.org/10.1101/820852>
76. Ivani I, Dans PD, Noy A, Pérez A, Faustino I, et al. 2016. Parmbsc1: a refined force field for DNA simulations. *Nat. Methods* 13:55–88
77. Izbicka E, Wheelhouse RT, Raymond E, Davidson KK, Lawrence RA, et al. 1999. Effects of cationic porphyrins as G-quadruplex interactive agents in human tumor cells. *Cancer Res.* 59:639–44
78. Jorgensen WL. 1981. Quantum and statistical mechanical studies of liquids. 10. Transferable intermolecular potential functions for water, alcohols, and ethers. Application to liquid water. *J. Am. Chem. Soc.* 103:335–40
79. Joung IS, Cheatham TE III. 2008. Determination of alkali and halide monovalent ion parameters for use in explicitly solvated biomolecular simulations. *J. Phys. Chem. B* 112:9020–41
80. Karim NHA, Mendoza O, Shivalingam A, Thompson AJ, Ghosh S, et al. 2014. Salphen metal complexes as tunable G-quadruplex binders and optical probes. *RSC Adv.* 4:3355–63
81. Keating L, Szalai V. 2004. Parallel-stranded guanine quadruplex interactions with a copper cationic porphyrin. *Biochemistry* 43:15891–900

82. Kieltyka R, Englebienne P, Fakhoury J, Autexier C, Moitessier N, Sleiman HF. 2008. A platinum supramolecular square as an effective G-quadruplex binder and telomerase inhibitor. *J. Am. Chem. Soc.* 130:10040–41
83. Kim MY, Vankayalapati H, Shin-Ya K, Wierzbka K, Hurley LH. 2002. Telomestatin, a potent telomerase inhibitor that interacts quite specifically with the human telomeric intramolecular G-quadruplex. *J. Am. Chem. Soc.* 124:2098–99
84. Kim NW, Piatyszek MA, Prowse KR, Harley CB, West MD, et al. 1994. Specific association of human telomerase activity with immortal cells and cancer. *Science* 266:2011–15
85. Klamt A. 1995. Conductor-like screening model for real solvents: a new approach to the quantitative calculation of solvation phenomena. *J. Phys. Chem.* 99:2224–35
86. Klamt A, Schüürmann G. 1993. Cosmo: a new approach to dielectric screening in solvents with explicit expressions for the screening energy and its gradient. *J. Chem. Soc.* 2:799–805
87. Kolesnikova S, Hubálek M, Bednářová L, Cvačka J, Curtis EA. 2017. Multimerization rules for G-quadruplexes. *Nucleic Acids Res.* 45:8684–96
88. Kostova I. 2006. Ruthenium complexes as anticancer agents. *Curr. Med. Chem.* 13:1085–107
89. Krepl M, Zgarbová M, Stadlbauer P, Otyepka M, Banas P, et al. 2012. Reference simulations of non-canonical nucleic acids with different χ variants of the AMBER force field: quadruplex DNA, quadruplex RNA, and Z-DNA. *J. Chem. Theory Comput.* 8:2506–20
90. Laio A, Parrinello M. 2002. Escaping free-energy minima. *PNAS* 99:12562–66
91. Le Grand S, Götz AW, Walker RC. 2013. SPFP: speed without compromise—a mixed precision model for GPU accelerated molecular dynamics simulations. *Comput. Phys. Commun.* 184:374–80
92. Lee W, Matsika S. 2015. QM/MM studies reveal pathways leading to the quenching of the formation of thymine dimer photoproduct by flanking bases. *Phys. Chem. Chem. Phys.* 17:9927–35
93. Lee W, Matsika S. 2017. Conformational and electronic effects on the formation of anti cyclobutane pyrimidine dimers in G-quadruplex structures. *Phys. Chem. Chem. Phys.* 19:3325–36
94. Levitt M, Warshel A. 1975. Computer simulation of protein folding. *Nature* 253:694–98
95. Li Q, Zhang J, Yang L, Yu Q, Chen Q, et al. 2014. Stabilization of G-quadruplex DNA and inhibition of telomerase activity studies of ruthenium(II) complexes. *J. Inorg. Biochem.* 130:122–29
96. Liao G, Chen X, Wu J, Qian C, Wang H, et al. 2014. Novel ruthenium(II) polypyridyl complexes as G-quadruplex stabilisers and telomerase inhibitors. *Dalton Trans.* 43:7811–19
97. Lim KW, Alberti P, Guédin A, Lacroix L, Riou J-F, et al. 2009. Sequence variation (CTAGGG)_n in the human telomere favors a G-quadruplex structure containing a G.C.G.C. tetrad. *Nucleic Acids Res.* 37:6239–48
98. Lim KW, Amrane S, Bouaziz S, Xu W, Mu Y, et al. 2009. Structure of the human telomere in K⁺ solution: a stable basket-type G-quadruplex with only two G-tetrad layers. *J. Am. Chem. Soc.* 131:4301–9
99. Limongelli V, De Tito S, Cerofolini L, Fragai M, Pagano B, et al. 2013. The G-triplex DNA. *Angew. Chem.* 125:2325–29
100. Liu W, Zhong YF, Liu LY, Shen CT, Zeng W, et al. 2018. Solution structures of multiple G-quadruplex complexes induced by a platinum(II)-based tripod reveal dynamic binding. *Nat. Commun.* 9:3496
101. Luu KN, Phan AT, Kuryavyy V, Lacroix L, Patel DJ. 2006. Structure of the human telomere in K⁺ solution: an intramolecular (3 + 1) G-quadruplex scaffold. *J. Am. Chem. Soc.* 128:9963–70
102. Lyubartsev A, Mirzoev A, Chen L, Laaksonen A. 2010. Systematic coarse-graining of molecular models by the Newton inversion method. *Faraday Discuss.* 144:43–56
103. Lyubartsev AP, Laaksonen A. 1995. Calculation of effective interaction potentials from radial distribution functions: a reverse Monte Carlo approach. *Phys. Rev. E* 52:3730–37
104. MacKerell AD Jr., Banavali N, Foloppe N. 2001. Development and current status of the CHARMM force field for nucleic acids. *Biopolymers* 56:257–65
105. Mandal SS, Varshney U, Bhattacharya S. 1997. Role of the central metal ion and ligand charge in the DNA binding and modification by metallosalen complexes. *Bioconjug. Chem.* 8:798–812
106. Marathias VM, Bolton PH. 2000. Structures of the potassium-saturated, 2:1, and intermediate, 1:1, forms of a quadruplex DNA. *Nucleic Acids Res.* 28:1969–77

107. Marathias VM, Wang KY, Kumar S, Pham TQ, Swaminathan S, Bolton PH. 1996. Determination of the number and location of the manganese binding sites of DNA quadruplexes in solution by EPR and NMR in the presence and absence of thrombin. *J. Mol. Biol.* 260:378–94
108. Maraval A, Franco S, Vialas C, Pratviel G, Blasco MA, Meunier B. 2003. Porphyrin–aminoquinoline conjugates as telomerase inhibitors. *Org. Biomol. Chem.* 1:921–27
109. Martino L, Virno A, Pagano B, Virgilio A, Di Micco S, et al. 2007. Structural and thermodynamic studies of the interaction of distamycin a with the parallel quadruplex structure [d(TGGGGT)]₄. *J. Am. Chem. Soc.* 129:16048–56
110. Mergny JL, Riou JF, Mailliet P, Teulade-Fichou MP, Gilson E. 2002. Natural and pharmacological regulation of telomerase. *Nucleic Acids Res.* 30:839–65
111. Minhas GS, Pilch DS, Kerrigan JE, LaVoie EJ, Rice JE. 2006. Synthesis and G-quadruplex stabilizing properties of a series of oxazole-containing macrocycles. *Bioorg. Med. Chem. Lett.* 16:3891–95
112. Mirzoev A, Lyubartsev AP. 2013. Magic: software package for multiscale modeling. *J. Chem. Theory Comput.* 9:1512–20
113. Mouret S, Baudouin C, Charveron M, Favier A, Cadet J, Douki T. 2006. Cyclobutane pyrimidine dimers are predominant DNA lesions in whole human skin exposed to UVA radiation. *PNAS* 103:13765–70
114. Nanda D, Jug K. 1980. SINDO1. A semiempirical SCF MO method for molecular binding energy and geometry I. Approximations and parametrization. *Theor. Chim. Acta* 57:95–106
115. Naome A, Laaksonen A, Vercauteren DP. 2014. A solvent-mediated coarse-grained model of DNA derived with the systematic Newton inversion method. *J. Chem. Theory Comput.* 10:3541–49
116. Neese F. 2012. ORCA—an ab initio, DFT and semiempirical SCF-MO package (version 2.9.1). *Software*. Univ. Bonn, Ger.
117. Ode H, Matsuo Y, Neya S, Hoshino T. 2008. Force field parameters for rotation around χ torsion axis in nucleic acids. *J. Comput. Chem.* 29:2531–42
118. Ordejón P, Artacho E, Soler JM. 1996. Self-consistent order-N density-functional calculations for very large systems. *Phys. Rev. B* 53:R10441–44
119. Pagano B, Fotticchia I, De Tito S, Mattia CA, Mayol L, et al. 2010. Selective binding of distamycin A derivative to G-quadruplex structure [d(TGGGT)]₄(4). *J. Nucleic Acids* 2010:247137
120. Pagano B, Virno A, Mattia CA, Mayol L, Randazzo A, Giancola C. 2008. Targeting DNA quadruplexes with distamycin A and its derivatives: an ITC and NMR study. *Biochimie* 90:1224–32
121. Pant M, Rajagopal A. 1972. Theory of inhomogeneous magnetic electron gas. *Solid State Commun.* 10:1157–60
122. Parkinson GN, Lee MP, Neidle S. 2002. Crystal structure of parallel quadruplexes from human telomeric DNA. *Nature* 417:876–80
123. Payne MC, Teter MP, Allan DC, Arias T, Joannopoulos AJ. 1992. Iterative minimization techniques for ab initio total-energy calculations: molecular dynamics and conjugate gradients. *Rev. Mod. Phys.* 64:1045
124. Perdew JP, Chevary JA, Vosko SH, Jackson KA, Pederson MR, et al. 1992. Atoms, molecules, solids, and surfaces: applications of the generalized gradient approximation for exchange and correlation. *Phys. Rev. B* 46:6671–87
125. Pérez A, Marchán I, Svozil D, Sponer J, Cheatham TE III, et al. 2007. Refinement of the AMBER force field for nucleic acids: improving the description of α/γ conformers. *Biophys. J.* 92:3817–29
126. Petraccone L, Fotticchia I, Cummaro A, Pagano B, Ginnari-Satriani L, et al. 2011. The triazatruxene derivative azatrux binds to the parallel form of the human telomeric G-quadruplex under molecular crowding conditions: biophysical and molecular modeling studies. *Biochimie* 93:1318–27
127. Phan AT, Kuryavii V, Luu KN, Patel DJ. 2007. Structure of two intramolecular G-quadruplexes formed by natural human telomere sequences in K⁺ solution. *Nucleic Acids Res.* 35:6517–25
128. Pople JA, Beveridge DL. 1970. *Approximate Molecular Orbital Theory*. New York: McGraw-Hill
129. Qin QP, Meng T, Tan MX, Liu YC, Luo XJ, et al. 2018. Synthesis and in vitro biological evaluation of three 4′-(4-methoxyphenyl)-2,2′:6′,2′′-terpyridine iridium(III) complexes as new telomerase inhibitors. *Eur. J. Med. Chem.* 143:1387–95
130. Randazzo A, Spada GP, da Silva MW. 2012. Circular dichroism of quadruplex structures. In *Quadruplex Nucleic Acids*, ed. JB Chaires, D Graves, pp. 67–86. Berlin: Springer

131. Rappe AK, Goddard WA III. 1991. Charge equilibration for molecular dynamics simulations. *J. Phys. Chem.* 95:3358–63
132. Rebic M, Mocci F, Laaksonen A, Ulicny J. 2014. Multiscale simulations of human telomeric G-quadruplex DNA. *J. Phys. Chem. B* 119:105–13
133. Rebic M, Mocci F, Ulicny J, Lyubartsev AP, Laaksonen A. 2017. Coarse-grained simulation of rodlike higher-order quadruplex structures at different salt concentrations. *ACS Omega* 2:386–96
134. Renčiuk D, Zhou J, Beaurepaire L, Guédin A, Bourdoncle A, Mergny JL. 2012. A fret-based screening assay for nucleic acid ligands. *Methods* 57:122–28
135. Reshetnikov RV, Sponer J, Rassokhina OI, Kopylov AM, Tsvetkov PO, et al. 2011. Cation binding to 15-TBA quadruplex DNA is a multiple-pathway cation-dependent process. *Nucleic Acids Res.* 39:9789–802
136. Rodriguez R, Muller S, Yeoman JA, Trentesaux C, Riou JF, Balasubramanian S. 2008. A novel small molecule that alters shelterin integrity and triggers a DNA-damage response at telomeres. *J. Am. Chem. Soc.* 130:15758–59
137. Romera C, Bombarde O, Bonnet R, Gomez D, Dumy P, et al. 2011. Improvement of porphyrins for G-quadruplex DNA targeting. *Biochimie* 93:1310–17
138. Rosu F, Gabelica V, Poncelet H, De Pauw E. 2010. Tetramolecular G-quadruplex formation pathways studied by electrospray mass spectrometry. *Nucleic Acids Res.* 38:5217–25
139. Ryckaert JP, Ciccotti G, Berendsen HJ. 1977. Numerical integration of the cartesian equations of motion of a system with constraints: molecular dynamics of *n*-alkanes. *J. Comput. Phys.* 23:327–41
140. Sabater L, Fang PJ, Chang CF, De Rache A, Prado E, et al. 2015. Cobalt(III) porphyrin to target G-quadruplex DNA. *Dalton Trans.* 44:3701–7
141. Sabharwal NC, Mendoza O, Nicoludis JM, Ruan T, Mergny JL, Yatsunyk LA. 2016. Investigation of the interactions between Pt(II) and Pd(II) derivatives of 5,10,15,20-tetrakis(N-methyl-4-pyridyl) porphyrin and G-quadruplex DNA. *J. Biol. Inorg. Chem.* 21:227–39
142. Sahakyan AB, Chambers VS, Marsico G, Santner T, Di Antonio M, Balasubramanian S. 2017. Machine learning model for sequence-driven DNA G-quadruplex formation. *Sci. Rep.* 7:14535
143. Salvati E, Leonetti C, Rizzo A, Scarsella M, Mottolose M, et al. 2007. Telomere damage induced by the G-quadruplex ligand RHPS4 has an antitumor effect. *J. Clin. Investig.* 117:3236–47
144. Scalmani G, Frisch MJ. 2010. Continuous surface charge polarizable continuum models of solvation. I. General formalism. *J. Chem. Phys.* 132:114110
145. Sen D, Gilbert W. 1988. Formation of parallel four-stranded complexes by guanine-rich motifs in DNA and its implications for meiosis. *Nature* 334:364–66
146. Senn HM, Thiel W. 2006. QM/MM methods for biological systems. In *Atomistic Approaches in Modern Biology: From Quantum Chemistry to Molecular Simulations*, ed. M Reiher, pp. 173–290. Berlin: Springer
147. Sherwood P, de Vries AH, Guest MF, Schreckenbach G, Catlow CRA, et al. 2003. QUASI: a general purpose implementation of the QM/MM approach and its application to problems in catalysis. *J. Mol. Struct. THEOCHEM* 632:1–28
148. Shi S, Geng X, Zhao J, Yao T, Wang C, et al. 2010. Interaction of [Ru(bpy)₂(dppz)]²⁺ with human telomeric DNA: preferential binding to G-quadruplexes over I-motif. *Biochimie* 92:370–77
149. Shin-ya K, Wierzbza K, Matsuo K, Ohtani T, Yamada Y, et al. 2001. Telomestatin, a novel telomerase inhibitor from *Streptomyces anulatus*. *J. Am. Chem. Soc.* 123:1262–63
150. Siddiqui-Jain A, Grand CL, Bearss DJ, Hurley LH. 2002. Direct evidence for a G-quadruplex in a promoter region and its targeting with a small molecule to repress c-MYC transcription. *PNAS* 99:11593–98
151. Smargiasso N, Rosu F, Hsia W, Colson P, Baker ES, et al. 2008. G-quadruplex DNA assemblies: loop length, cation identity, and multimer formation. *J. Am. Chem. Soc.* 130:10208–16
152. Smith JE, Lu C, Taylor JS. 2014. Effect of sequence and metal ions on UVB-induced anti cyclobutane pyrimidine dimer formation in human telomeric DNA sequences. *Nucleic Acids Res.* 42:5007–19
153. Soder JM, Artacho E, Gale JD, Garca A, Junquera J, et al. 2002. The SIESTA method for ab initio order-N materials simulation. *J. Phys. Condensed Matter* 14:2745–79
154. Soper A. 1996. Empirical potential Monte Carlo simulation of fluid structure. *Chem. Phys.* 202:295–306

155. Šponer J, Mladek A, Spackova N, Cang X, Cheatham TE III, Grimme S. 2013. Relative stability of different DNA guanine quadruplex stem topologies derived using large-scale quantum-chemical computations. *J. Am. Chem. Soc.* 135:9785–96
156. Stadlbauer P, Krepl M, Cheatham TE, Koča J, Šponer J. 2013. Structural dynamics of possible late-stage intermediates in folding of quadruplex DNA studied by molecular simulations. *Nucleic Acids Res.* 41:7128–43
157. Stadlbauer P, Mazzanti L, Cragolini T, Wales DJ, Derreumaux P, et al. 2016. Coarse-grained simulations complemented by atomistic molecular dynamics provide new insights into folding and unfolding of human telomeric G-quadruplexes. *J. Chem. Theory Comput.* 12:6077–97
158. Stadlbauer P, Trantrek L, Cheatham TE III, Koča J, Šponer J. 2014. Triplex intermediates in folding of human telomeric quadruplexes probed by microsecond-scale molecular dynamics simulations. *Biochimie* 105:22–35
159. Staroverov VN, Scuseria GE, Tao J, Perdew JP. 2003. Comparative assessment of a new nonempirical density functional: molecules and hydrogen-bonded complexes. *J. Chem. Phys.* 119:12129–37
160. Štefl R, Cheatham TE III, Špačková N, Fadrná E, Berger I, et al. 2003. Formation pathways of a guanine-quadruplex DNA revealed by molecular dynamics and thermodynamic analysis of the substrates. *Biophys. J.* 85:1787–804
161. Stewart JJ. 1989. Optimization of parameters for semiempirical methods. II. Applications. *J. Comput. Chem.* 10:221–64
162. Su DG, Fang H, Gross ML, Taylor JSA. 2009. Photocrosslinking of human telomeric G-quadruplex loops by anti cyclobutane thymine dimer formation. *PNAS* 106:12861–66
163. Sun RWY, Li CKL, Ma DL, Yan JJ, Lok CN, et al. 2010. Stable anticancer gold(III)–porphyrin complexes: effects of porphyrin structure. *Chem. Eur. J.* 16:3097–113
164. te Velde G, Bickelhaupt FM, Baerends EJ, Fonseca Guerra C, van Gisbergen JA, et al. 2001. Chemistry with ADF. *J. Comput. Chem.* 22:931–67
165. Terenzi A, Bonsignore R, Spinello A, Gentile C, Martorana A, et al. 2014. Selective G-quadruplex stabilizers: Schiff-base metal complexes with anticancer activity. *RSC Adv.* 4:33245–56
166. Terenzi A, Lötsch D, van Schoonhoven S, Roller A, Kowol CR, et al. 2016. Another step toward DNA selective targeting: Ni(II) and Cu(II) complexes of a Schiff base ligand able to bind gene promoter G-quadruplexes. *Dalton Trans.* 45:7758–67
167. Tuntiwechapikul W, Lee JT, Salazar M. 2001. Design and synthesis of the G-quadruplex-specific cleaving reagent perylene-EDTA.iron(II). *J. Am. Chem. Soc.* 123:5606–7
168. Tuntiwechapikul W, Salazar M. 2001. Cleavage of telomeric G-quadruplex DNA with perylene-EDTA.Fe(II). *Biochemistry* 40:13652–58
169. Varizhuk AM, Protopopova AD, Tsvetkov VB, Barinov NA, Podgorsky VV, et al. 2018. Polymorphism of G4 associates: from stacks to wires via interlocks. *Nucleic Acids Res.* 46:8978–92
170. Vialas C, Pratviel G, Meunier B. 2000. Oxidative damage generated by an oxo-metalloporphyrin onto the human telomeric sequence. *Biochemistry* 39:9514–22
171. Wang Y, Patel DJ. 1993. Solution structure of the human telomeric repeat d[AG3(T2AG3)3] G-tetraplex. *Structure* 1:263–82
172. Warshel A, Levitt M. 1976. Theoretical studies of enzymic reactions: dielectric, electrostatic and steric stabilization of the carbonium ion in the reaction of lysozyme. *J. Mol. Biol.* 103:227–49
173. Weigend F, Ahlrichs R. 2005. Balanced basis sets of split valence, triple zeta valence and quadruple zeta valence quality for H to Rn: design and assessment of accuracy. *Phys. Chem. Chem. Phys.* 7:3297–305
174. Wolters LP, Smits NW, Guerra CF. 2015. Covalency in resonance-assisted halogen bonds demonstrated with cooperativity in N-halo-guanine quartets. *Phys. Chem. Chem. Phys.* 17:1585–92
175. Wu P, Ma DL, Leung CH, Yan SC, Zhu N, et al. 2009. Stabilization of G-quadruplex DNA with platinum(II) Schiff base complexes: luminescent probe and down-regulation of C-Myc oncogene expression. *Chem. Eur. J.* 15:13008–21
176. Xia Y, Chen Q, Qin X, Sun D, Zhang J, Liu J. 2013. Studies of ruthenium(II)-2,2'-bisimidazole complexes on binding to G-quadruplex DNA and inducing apoptosis in HeLa cells. *New J. Chem.* 37:3706–15

177. Xu CX, Shen Y, Hu Q, Zheng YX, Cao Q, et al. 2014. Stabilization of human telomeric G-quadruplex and inhibition of telomerase activity by propeller-shaped trinuclear Pt(II) complexes. *Chem. Asian J.* 9:2519–26
178. Xu CX, Zheng YX, Zheng XH, Hu Q, Zhao Y, et al. 2013. V-shaped dinuclear Pt(II) complexes: selective interaction with human telomeric G-quadruplex and significant inhibition towards telomerase. *Sci. Rep.* 3:2060
179. Xu Y, Suzuki Y, Lonnberg T, Komiyama M. 2009. Human telomeric DNA sequence-specific cleaving by G-quadruplex formation. *J. Am. Chem. Soc.* 131:2871–74
180. Yao JL, Gao X, Sun W, Shi S, Yao TM. 2013. [Ru(bpy)₂dppz-idzo]²⁺: a colorimetric molecular “light switch” and powerful stabilizer for G-quadruplex DNA. *Dalton Trans.* 42:5661–72
181. You YH, Lee DH, Yoon JH, Nakajima S, Yasui A, Pfeifer GP. 2001. Cyclobutane pyrimidine dimers are responsible for the vast majority of mutations induced by UVB irradiation in mammalian cells. *J. Biol. Chem.* 276:44688–94
182. Zaccaria F, Fonseca Guerra C. 2018. RNA versus DNA G-quadruplex: the origin of increased stability. *Chem. Eur. J.* 24:16315–22
183. Zaccaria F, Paragi G, Guerra CF. 2016. The role of alkali metal cations in the stabilization of guanine quadruplexes: why K⁺ is the best. *Phys. Chem. Chem. Phys.* 18:20895–904
184. Zerner M. 1991. Semiempirical molecular orbital methods. In *Reviews in Computational Chemistry*, Vol. 2, ed. KB Lipkowitz, DB Boyd, pp. 313–65. Hoboken, NJ: Wiley
185. Zgarbová M, Sponer J, Otyepka M, Cheatham TE III, Galindo-Murillo R, Jurecka P. 2015. Refinement of the sugar–phosphate backbone torsion beta for AMBER force fields improves the description of Z- and B-DNA. *J. Chem. Theory Comput.* 11:5723–36
186. Zhou J, Bourdoncle A, Rosu F, Gabelica V, Mergny JL. 2012. Tri-G-quadruplex: controlled assembly of a G-quadruplex structure from three G-rich strands. *Angew. Chem. Int. Ed.* 51:11002–5

Contents

Review of COVID-19 Antibody Therapies <i>Jiabui Chen, Kaifu Gao, Rui Wang, Duc Duy Nguyen, and Guo-Wei Wei</i>	1
The Mechanosensory Transduction Machinery in Inner Ear Hair Cells <i>Wang Zheng and Jeffrey R. Holt</i>	31
Structure of Phycobilisomes <i>Sen-Fang Sui</i>	53
Biophysics of Chromatin Remodeling <i>Ilana M. Nodelman and Gregory D. Bowman</i>	73
Structures and Functions of Chromatin Fibers <i>Ping Chen, Wei Li, and Guobong Li</i>	95
From Bench to Keyboard and Back Again: A Brief History of Lambda Phage Modeling <i>Michael G. Cortes, Yiruo Lin, Lanying Zeng, and Gábor Balázs</i>	117
Recent Developments in the Field of Intrinsically Disordered Proteins: Intrinsic Disorder–Based Emergence in Cellular Biology in Light of the Physiological and Pathological Liquid–Liquid Phase Transitions <i>Vladimir N. Uversky</i>	135
Biophysics of Notch Signaling <i>David Sprinzak and Stephen C. Blacklow</i>	157
Bayesian Inference: The Comprehensive Approach to Analyzing Single-Molecule Experiments <i>Colin D. Kinz-Thompson, Korak Kumar Ray, and Ruben L. Gonzalez Jr.</i>	191
Learning to Model G-Quadruplexes: Current Methods and Perspectives <i>Iker Ortiz de Luzuriaga, Xabier Lopez, and Adrià Gil</i>	209
Analysis of Tandem Repeat Protein Folding Using Nearest-Neighbor Models <i>Mark Petersen and Doug Barrick</i>	245

Biomolecular Modeling and Simulation: A Prospering Multidisciplinary Field <i>Tamar Schlick, Stephanie Portillo-Ledesma, Christopher G. Myers, Lauren Beljak, Justin Chen, Sami Dakbel, Daniel Darling, Sayak Ghosh, Joseph Hall, Mikael Jan, Emily Liang, Sera Saju, Mackenzie Vöhr, Chris Wu, Yifan Xu, and Eva Xue</i>	267
Biomolecular Systems Engineering: Unlocking the Potential of Engineered Allostery via the Lactose Repressor Topology <i>Thomas M. Groseclose, Ronald E. Rondon, Ashley N. Hersey, Prasaad T. Milner, Dowan Kim, Fumin Zhang, Matthew J. Reaff, and Corey J. Wilson</i>	303
Directed Evolution of Microbial Communities <i>Álvaro Sánchez, Jean C.C. Vila, Chang-Yu Chang, Juan Diaz-Colunga, Sylvie Estrela, and María Rebolleda-Gomez</i>	323
The Molecular Basis for Life in Extreme Environments <i>Nozomi Ando, Blanca Barquera, Douglas H. Bartlett, Eric Boyd, Audrey A. Burnim, Amanda S. Byer, Daniel Colman, Richard E. Gillilan, Martin Gruebele, George Makhatadze, Catherine A. Royer, Everett Shock, A. Joshua Wand, and Maxwell B. Watkins</i>	343
The Sliding Filament Theory Since Andrew Huxley: Multiscale and Multidisciplinary Muscle Research <i>Joseph D. Powers, Sage A. Malingen, Michael Regnier, and Thomas L. Daniel</i>	373
How Physical Interactions Shape Bacterial Biofilms <i>Berenike Maier</i>	401
Cutting-Edge Single-Molecule Technologies Unveil New Mechanics in Cellular Biochemistry <i>Souradeep Banerjee, Sobam Chakraborty, Abhijit Sreepada, Devshuvam Banerji, Shashwat Goyal, Yajushi Khurana, and Shubbasis Haldar</i>	419
Measuring Absolute Membrane Potential Across Space and Time <i>Julia R. Lazzari-Dean, Anneliese M.M. Gest, and Evan W. Miller</i>	447
Advancing Biophysics Using DNA Origami <i>Wouter Engelen and Hendrik Dietz</i>	469
The Contribution of Biophysics and Structural Biology to Current Advances in COVID-19 <i>Francisco J. Barrantes</i>	493
Protein Reconstitution Inside Giant Unilamellar Vesicles <i>Thomas Litschel and Petra Schwille</i>	525
Structure and Mechanics of Dynein Motors <i>John T. Canty, Ruensern Tan, Emre Kusakci, Jonathan Fernandes, and Ahmet Yildiz</i>	549

The Phasor Plot: A Universal Circle to Advance Fluorescence Lifetime
Analysis and Interpretation
Leonel Malacrida, Suman Ranjit, David M. Jameson, and Enrico Gratton 575

Molecular Force Measurement with Tension Sensors
Lisa S. Fischer, Srishti Rangarajan, Tanmay Sadbanasatish, and Carsten Grashoff 595

Indexes

Cumulative Index of Contributing Authors, Volumes 46–50 617

Errata

An online log of corrections to *Annual Review of Biophysics articles* may be found at
<http://www.annualreviews.org/errata/biophys>